

An Information Theoretic Evaluation Metric for Strong Unlearning

Dongjae Jeon^{1*}, Wonje Jeung^{2*}, Taeheon Kim³, Albert No^{2†}, Jonghyun Choi^{3,4,5†}

¹Department of Computer Science, Yonsei University

²Department of Artificial Intelligence, Yonsei University

³ECE, ⁴IPAI and ⁵ASRI, Seoul National University

{dongjae0324, specific0924, albertno}@yonsei.ac.kr, {thkim0305, jonghyunchoi}@snu.ac.kr

Abstract

Machine unlearning (MU) aims to remove the influence of specific data from trained models, addressing privacy concerns and ensuring compliance with regulations such as the “right to be forgotten.” Evaluating strong unlearning, where the unlearned model is indistinguishable from one retrained without the forgetting data, remains a significant challenge in deep neural networks (DNNs). Common black-box metrics, such as variants of membership inference attacks and accuracy comparisons, primarily assess model outputs but often fail to capture residual information in intermediate layers. To bridge this gap, we introduce the Information Difference Index (IDI), a novel white-box metric inspired by information theory. IDI quantifies retained information in intermediate features by measuring mutual information between those features and the labels to be forgotten, offering a more comprehensive assessment of unlearning efficacy. Our experiments demonstrate that IDI effectively measures the degree of unlearning across various datasets and architectures, providing a reliable tool for evaluating strong unlearning in DNNs.

1 Introduction

Machine unlearning (MU) seeks to remove the impact of specific data samples from a trained model, addressing privacy issues such as “right to be forgotten” (Voigt and Von dem Bussche 2017). In addition to privacy, MU is also emerging as a tool to eliminate the influence of corrupted or outdated data used during training (Nguyen et al. 2022; Kurmanji et al. 2023). The most straightforward approach to MU is *exact unlearning*, where the model is retrained from scratch, excluding the data that need to be forgotten. Although this method ensures complete data removal, it is computationally expensive and not scalable (Aldaghri, Mahdaviifar, and Beirami 2021; Bourtoule et al. 2021). Consequently, research has shifted towards *approximate unlearning*, which aims to replicate the effects of retraining in a more efficient manner.

The goal of MU is to create an unlearned model that is indistinguishable from a model retrained from scratch, referred to as strong unlearning. This objective has become

particularly crucial with the rise of open-source models like Stable Diffusion (Rombach et al. 2022) and LLaMA (Touvron et al. 2023), which are widely used and fine-tuned by various users. For unlearning algorithms to be practically useful, they must be capable of fully eliminating traces of private data and preventing potential exploitation. While (ϵ, δ) -certified unlearning methods (Zhang et al. 2024b; Mu and Klabjan 2024) provide theoretical guarantees, they are impractical for large-scale models. As a result, most approximate unlearning methods rely on heuristic approaches, lacking formal guarantees. Thus, these methods must undergo empirical evaluation to demonstrate their effectiveness.

However, current evaluations, primarily based on black-box approaches such as membership inference attacks (MIA) (Shokri et al. 2017) and accuracy comparisons, focus on output similarity rather than internal model changes. Although these metrics may capture weak unlearning (Fan et al. 2024; Jia et al. 2023; Chundawat et al. 2023a), they may not be sufficient for assessing strong unlearning. In this work, we investigate whether relying solely on outputs can truly reflect complete influence removal, considering that model outputs can be superficially adjusted (Kirichenko, Izmailov, and Wilson 2023).

Surprisingly, our experiments reveal that even minimal changes to the model, such as modifying only the final layer while preserving all information in the intermediate layers, can still satisfy the black-box evaluation metrics, exposing their limitations in assessing strong unlearning. This finding also raises critical concerns about whether current MU methods genuinely achieve information removal comparable to retraining from scratch.

Consequently, motivated by the Information Bottleneck principle (Tishby, Pereira, and Bialek 2000; Tishby and Zaslavsky 2015), we introduce the **information difference index (IDI)**, a novel white-box metric designed to quantify residual information in intermediate layers after unlearning. IDI measures the mutual information (Shannon 1948) between intermediate features and the forgetting labels, providing an interpretable value to assess the effectiveness of unlearning algorithms. We observe that IDI remains stable under the stochasticity of the unlearning process and is compatible with diverse model architectures. Moreover, IDI can be reliably estimated from a data subset, making it practical for large-scale unlearning settings.

*These authors contributed equally.

†Corresponding authors.

Through IDI, we observe that many recent MU methods, despite strong performance on black-box metrics, retain substantial information about the forgetting data in intermediate layers. To address this, we propose **COLapse-and-Align (COLA)**, a simple method that collapses representations associated with the forget set at the feature level to eliminate residual information, followed by re-aligning the retained features. Despite its simplicity, COLA consistently improves IDI scores while maintaining competitive performance across datasets such as CIFAR-10/100, and ImageNet-1K, and architectures (ResNet-18/50, ViT).

2 Problem Statement and Preliminaries

2.1 Problem Statement

Let $D = \{(x_i, y_i)\}_{i=1}^N$ denote a training dataset comprising N image-label pairs (x_i, y_i) . In a supervised learning setup, D is partitioned into two subsets: the *forget set* D_f , containing the data points to be removed, and the *retain set* $D_r = D \setminus D_f$, containing the data points to be preserved. The initial model θ_o , referred to as the **Original model**, is trained on the full dataset D using empirical risk minimization. The **Retrain model** θ_r is trained from scratch on only the retain set D_r . The **unlearned model** θ_u is obtained by applying a MU algorithm to the Original model θ_o , aiming to remove the influence of D_f . The goal of MU is for θ_u to closely approximate θ_r , ensuring the unlearned model behaves as though D_f had never been used in training, while preserving the training methodology across θ_o , θ_r , and θ_u .

Throughout the paper, within a given model θ , we define the **head** as the last few layers responsible for classification; typically one to three linear layers. The **encoder**, on the contrary, encompasses the remainder of the network, which usually consists of convolutional layers or transformer encoders. MU is often studied in the context of image classification (Shaik et al. 2023; Nguyen et al. 2022), where it is typically classified into two scenarios based on the nature of the forget set: **class-wise forgetting**, where all samples from a specific class are targeted, and **random data forgetting**, where samples are selected indiscriminately across all classes. In this work, we tackle both scenarios.

2.2 Preliminaries

Machine Unlearning (MU). Exact unlearning, which involves creating Retrain, guarantees the information removal from the forget set but is computationally expensive (Bourtoule et al. 2021; Yan et al. 2022). To address this, approximate unlearning methods have been developed, focusing on efficiency rather than strict theoretical guarantees. Specifically, strong unlearning, where the unlearned model is indistinguishable from Retrain, has been explored through the application of differential privacy (DP) (Dwork and Roth 2014) inspired techniques, which aim to achieve parameter-level indistinguishability (Dwork and Roth 2014; Neel, Roth, and Sharifi-Malvajerdi 2021; Sekhari et al. 2021). However, applying such techniques to neural networks remains challenging due to their vast number of parameters and non-convex loss landscapes (Qiao et al. 2024). As a result, recent studies typically assess the similarity of

model outputs (i.e., predictions), using weak unlearning as a practical proxy for strong unlearning (Xu et al. 2023).

Although empirically ensuring strong unlearning is challenging, it remains essential for deploying unlearning algorithms in compliance with legal requirements such as the GDPR (Voigt and Von dem Bussche 2017) and the “right to be forgotten.” This need is further amplified by the widespread use of open-source models like CLIP (Radford et al. 2021), Stable Diffusion (Rombach et al. 2022), and LLaMA (Touvron et al. 2023), where sensitive data may inadvertently persist and be exploited. Our work focuses on developing a robust empirical metric to evaluate unlearning algorithms, distinct from verification (Zhang et al. 2024a; Sommer et al. 2022), which assesses effectiveness through real-world attack scenarios.

Evaluation Criteria in MU. As the goal of MU is to remove the influence of specific data while preserving the others, the unlearning algorithms are typically evaluated on three criteria: *Efficacy*, *Accuracy*, and *Efficiency* (Hayes et al. 2024). Efficacy measures how closely the unlearned model approximates Retrain, which is key to unlearning quality. Accuracy ensures task performance remains intact after unlearning, while efficiency ensures the unlearning process is faster than retraining.

Accuracy and efficiency can be easily evaluated using existing metrics. Accuracy consists of three categories: *unlearning accuracy (UA)*, *remaining accuracy (RA)*, and *testing accuracy (TA)*. UA measures performance on \mathcal{D}_f as $UA(\theta_u) = 1 - \text{Acc}_{\mathcal{D}_f}(\theta_u)$, RA on \mathcal{D}_r as $RA(\theta_u) = \text{Acc}_{\mathcal{D}_r}(\theta_u)$, and TA measures generalization to unseen data as $TA(\theta_u) = \text{Acc}_{\mathcal{D}_{test}}(\theta_u)$. Performance levels comparable to Retrain across these metrics indicate better unlearning.

In terms of efficiency, *runtime efficiency (RTE)* measures the time an algorithm takes to complete unlearning, with lower RTE indicating more efficient unlearning (Fan et al. 2024; Jia et al. 2023). However, assessing unlearning efficacy, or determining whether the unlearned model has fully removed the influence of specific data to the same extent as Retrain, remains a significant challenge in complex DNNs. The efficacy metrics are divided into two categories: *black-box* metrics, which focus solely on model outputs (i.e., predictions), and *white-box* metrics, which examine internal dynamics such as parameters, gradients, and features. While black-box metrics are typically used due to their convenience, no universally accepted standard exists, leaving room for more reliable assessment.

Black-box Efficacy Metrics. Variants of membership inference attacks (MIA) (Shokri et al. 2017) are among the most widely used black-box metrics for evaluating unlearning (Fan et al. 2024; Jia et al. 2023; Foster, Schoepf, and Brintrup 2024). MIA trains an auxiliary classifier to determine whether a given sample was part of the training set, with attack success rates on the forget set close to those for Retrain being preferred in unlearning. Recent studies often combine MIA with UA, RA, TA, and RTE to assess unlearning across efficacy, accuracy, and efficiency (Chen et al. 2023; Kim, Lee, and Woo 2024), a practice referred to as the ‘full-stack’ evaluation (Jia et al. 2023; Fan et al. 2024).

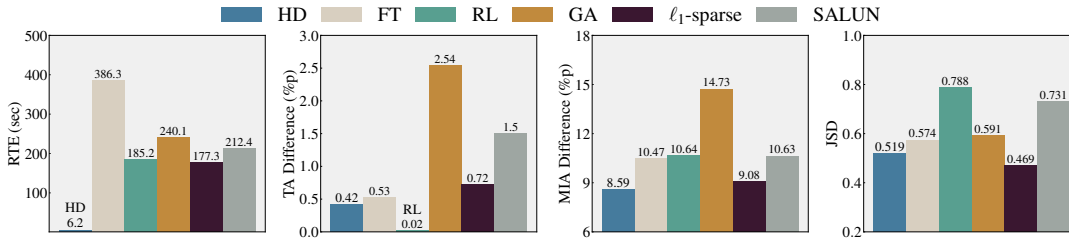


Figure 1: Performance of six methods on (CIFAR-10, ResNet-18), evaluated in efficiency (RTE), accuracy (TA), and efficacy (MIA, JSD). For TA, MIA, and JSD, lower differences from Retrain are preferred, indicating closer similarity to Retrain.

Other metrics, such as Jensen-Shannon divergence (JSD), and ZRF (Chundawat et al. 2023a; Poppi et al. 2024) compare the output logits between the unlearned model and Retrain (or a random model for ZRF). Additionally, time-based metrics like Anamnesis Index (AIN) (Chundawat et al. 2023b; Tarun et al. 2023a) and relearn time (RT) (Tarun et al. 2023b) track how long the model takes to regain performance on the forget set. While convenient, black-box metrics overlook internal behaviors and cannot verify strong unlearning by ensuring forgetting data’s influence is fully removed. Their limitations are further discussed in Section 3.

White-box Efficacy Metrics. In contrast, white-box metrics offer deeper insights by analyzing internal model dynamics. Previous studies have measured parameter-wise distances (e.g., ℓ_2 -distance, KL-divergence) between the unlearned model and Retrain (Golatkar, Achille, and Soatto 2020; Wu, Dobriban, and Davidson 2020). However, this approach is computationally expensive and unreliable due to training randomness (Hayes et al. 2024; Goel et al. 2022). Becker and Liebig (2022) proposed a Fisher information based metric, but their results were inconsistent with theoretical intuition. Graves, Nagisetty, and Ganesh (2021) applied model inversion attacks to reconstruct images from the forget set, but their method relies on visual comparisons.

Although robust white-box metrics are currently lacking and challenging to develop, they are crucial for validating approximate methods that lack formal guarantees. Without them, these algorithms cannot be trusted in privacy-sensitive applications that demand a high level of confidence in information removal. To address this critical need, our work proposes a reliable and practical white-box metric.

3 Rethinking the Evaluation of Unlearning

3.1 Challenging Black-box Metrics

In this section, we reveal the limitations of commonly used black-box efficacy metrics by applying a simple unlearning technique to a single-class forgetting task. We show that these metrics can misrepresent unlearning efficacy, even when the model’s output closely resembles that of Retrain.

Inspired by the teacher-student framework, our strategy, termed **head distillation (HD)**, employs logit distillation from Original θ_o . The unlearned model θ_u is initialized from θ_o with the encoder frozen and only the head trainable. During unlearning, the head is finetuned on training dataset \mathcal{D} using KL-divergence loss (Hinton, Vinyals, and Dean 2014)

to match a masked version of θ_o ’s output, where the logit for the forgetting class is set to negative infinity. This approach enables θ_u to mimic a pseudo-retrained model, as the masked logits closely resemble those of Retrain. By aligning output behavior, HD approximates the intended unlearning effect. Detailed explanation is available at Section C.1.

We evaluated HD on CIFAR-10 (Krizhevsky 2009) using ResNet-18 (He et al. 2016), where the head is only a single linear layer. For *efficacy*, we used membership inference attack (MIA) and Jensen-Shannon divergence (JSD). For *accuracy* and *efficiency*, we measured unlearning accuracy (UA), testing accuracy (TA), and run-time efficiency (RTE). See Section C.2 for metric details. We compared HD with recent methods, including FT, RL (Golatkar, Achille, and Soatto 2020), GA (Thudi et al. 2022), ℓ_1 -sparse (Jia et al. 2023), and SALUN (Fan et al. 2024). Details on the baselines can be found in Section C.3.

Figure 1 shows the experimental results. Despite its simplicity, HD outperforms all other methods in MIA and ranking second in JSD. HD achieves this performance in just 6.2 seconds, approximately 30 to 60 times faster than competing methods. Additionally, HD maintains comparable testing accuracy (TA), effectively preserving task performance. All methods achieved perfect unlearning accuracy (100% UA), which is omitted from Figure 1. Notably, HD’s strong performance generalize to multi-class and random data forgetting, as shown in Section D.1.

The results indicate that HD performs exceptionally well across all black-box metrics. However, its validity as a MU algorithm requires scrutiny. The primary issue is that HD closely resembles Original θ_o , with changes limited to the single-layer head, while the encoder remains identical to θ_o . Consequently, all intermediate features related to the forget set are perfectly retained. This raises a critical question:

Do black-box metrics truly capture the unlearning quality, or are they misled by superficial changes while deeper information persists?

3.2 Residual Information of Forgetting Data

To address the above question, we analyze recent unlearning methods to assess whether they internally remove information from the forget set, despite their strong performance on black-box metrics. Note that analyses use the same experimental setup described in Section 3.1.

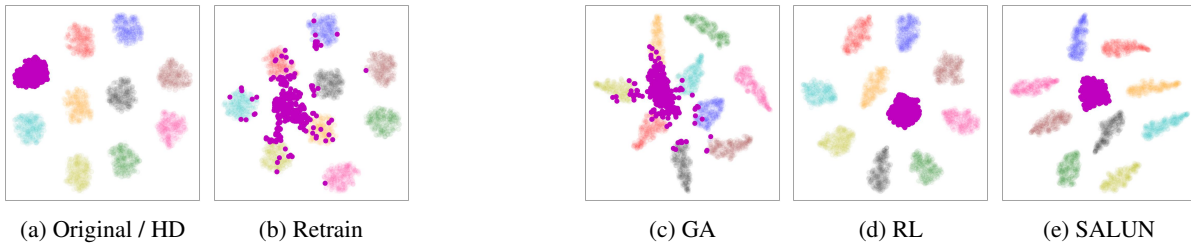


Figure 2: t-SNE visualizations of encoder outputs for Original, Retrain, and unlearned models from three MU methods (GA, RL, SALUN) on single-class forgetting with (CIFAR-10, ResNet-18). In each t-SNE plot, features of the forgetting class are represented in purple. Original and HD have identical feature distribution as they share the same encoder.

We begin with a qualitative analysis using t-SNE (van der Maaten and Hinton 2008) visualizations of intermediate features from model encoders to compare Retrain and Original, and to examine internal behaviors of unlearning methods (Figure 2). In Figure 2b, the forgetting class (in purple) shows a scattered distribution in Retrain, indicating difficulty in forming coherent representations. This scattering reflects an desirable outcome of strong unlearning, suggesting that the model has successfully ‘forgotten’ how to encode meaningful semantic information from the forget set.

Notably, while the features from GA (Thudi et al. 2022) appear scattered in a manner similar to Retrain, the features from RL (Golatkar, Achille, and Soatto 2020) and SALUN (Fan et al. 2024) closely resemble those of Original. In addition, HD, which shares the same encoder as Original, shows identical t-SNE results. These findings indicate that several unlearned models still retain a significant capacity to recognize the forgetting class, unlike Retrain.

After training, we evaluated the accuracy of the new models on the forget test data. Surprisingly, as shown in Figure 3, while the retrained head of Retrain achieves no more than 41% accuracy, the heads from certain methods, like Bad-T, SALUN, and RL exhibit over 82% accuracy. Notably, the high accuracy observed in SALUN and RL aligns with their clustered t-SNE patterns in Figure 2.

The results from the above analyse demonstrate that unlearned models across various MU algorithms retain substantial residual influence from the forget set, indicating incomplete unlearning. Critically, standard black-box metrics fail to capture these internal traces. If such metrics cannot ensure strong unlearning, the reliability of approximate unlearning algorithms, which often lack theoretical guarantees, becomes questionable in real world applications. Therefore, developing practical white box approaches that consider internal model behaviors is essential to achieving the fundamental goal of unlearning.

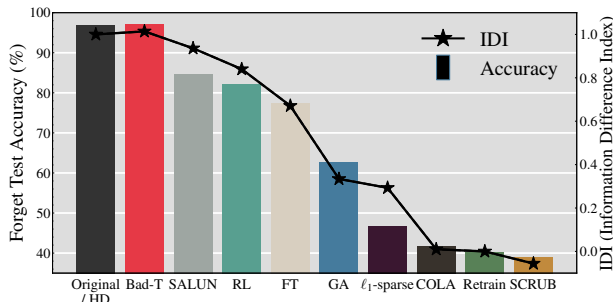


Figure 3: Forget test accuracy and IDI (our metric in Section 4.3) for Original, Retrain, and MU methods (including COLA, our method in Section 5.1) after head retraining with fixed unlearned encoders using 2% of \mathcal{D} in (CIFAR-10, ResNet-18). IDI aligns with the recovered accuracy.

To further examine the residual influence in unlearned models, we conducted a follow-up experiment inspired by time-based metrics (e.g., Chundawat et al. (2023b)). We test whether unlearned encoders can recover forgotten information using minimal data. Specifically, we replaced the heads of all models, including Retrain and Original, with randomly initialized ones. The encoders were then frozen, and new heads were trained on \mathcal{D}' , a small subset (only 2% of the total) of \mathcal{D} sampled at random.

4 An Information Theoretic Metric

Black-box metrics often overlook residual information in intermediate layers, as shown in Section 3. To address this, we measure residual information in the intermediate features of unlearned models using mutual information. Building on this, we propose a novel white-box metric, IDI, that goes beyond output-based evaluations.

4.1 Quantifying Residual Information

To quantify the relationship between intermediate features and data labels, we utilize Shannon’s mutual information (MI), a robust measure that captures variable dependencies across dimensional complexities. For an input \mathbf{X} , let $\mathbf{Z}_\ell^{(u)}$ and $\mathbf{Z}_\ell^{(r)}$ denote the features from the ℓ -th layer of the total L -layer encoder in the unlearned model and Retrain, respectively. Let Y be a binary label indicating whether \mathbf{X} belongs to the forget set ($Y = 1$) or not ($Y = 0$). We compute MI $I(\mathbf{Z}_\ell; Y)$ across each layer from 1 to L , to determine whether intermediate features retain information about the forget set. For estimation, we adopt the InfoNCE loss (Oord, Li, and Vinyals 2018), a robust method widely used in deep MI estimation (Radford et al. 2021; Jia et al. 2021).

Given a batch $\mathcal{B} = \{(U^{(k)}, V^{(k)}) : 1 \leq k \leq K\}$, sampled from a joint distribution $P_{U,V}$, where $U \in \mathcal{U}$ and $V \in \mathcal{V}$ be random variables. The InfoNCE loss (Poole et al. 2019) is

defined as:

$$\mathcal{L}_{\text{NCE}} = \frac{1}{K} \sum_{k=1}^K \log \frac{\exp(f_{\nu}(U^{(k)})^{\top} g_{\eta}(V^{(k)}))}{\frac{1}{K} \sum_{k'=1}^K \exp(f_{\nu}(U^{(k)})^{\top} g_{\eta}(V^{(k')}))},$$

where $f_{\nu} : \mathcal{U} \rightarrow \mathbb{R}^d$ and $g_{\eta} : \mathcal{V} \rightarrow \mathbb{R}^d$ are critic functions, with an output embedding dimension d , parameterized by neural networks with parameters ν and η . This neural network parameterization, inspired by Radford et al. (2021), effectively captures complex relationships in contrastive learning through flexible and expressive modeling of the joint distributions of U and V .

The InfoNCE loss serves as a lower bound on the MI between U and V . In fact, the maximum value of the InfoNCE loss, when using the joint critic functions, equals the mutual information:

$$I(U; V) = \max_{\nu, \eta} \mathcal{L}_{\text{NCE}}(\mathcal{B}, \nu, \eta).$$

By maximizing this loss over parameters ν and η through neural networks, we effectively capture data structure and accurately quantify shared information between U and V .

To estimate mutual information (MI) at each layer, we define separate critic functions for every layer: $f_{\nu_{\ell}}$ and $g_{\eta_{\ell}}$, where $\ell \in \{1, \dots, L\}$ denotes the layer index. The critic $g_{\eta_{\ell}}$ models the binary variable Y as two trainable d -dimensional vectors, $g_{\eta_{\ell}}(0)$ and $g_{\eta_{\ell}}(1)$, selecting the appropriate one based on the value of Y . In parallel, $f_{\nu_{\ell}}$ maps intermediate features \mathbf{Z}_{ℓ} from the ℓ -th encoder layer to a shared d -dimensional embedding space. The parameters ν_{ℓ} define the weights and biases of this neural network.

The complexity of $f_{\nu_{\ell}}$ depends on the layer depth: in earlier layers, $f_{\nu_{\ell}}$ processes raw, less interpretable features, requiring a more intricate design to capture the relationship between \mathbf{Z}_{ℓ} and Y . In later layers, with more structured features, $f_{\nu_{\ell}}$ can perform the mapping more directly. This design enables the accurate estimation of $I(\mathbf{Z}_{\ell}; Y)$, capturing the dependency between features and labels at different depths. For details on $f_{\nu_{\ell}}$ and $g_{\eta_{\ell}}$, refer to Section B.

To achieve a model-agnostic design, we construct $f_{\nu_{\ell}}$ by reusing the network layers from $\ell + 1$ to L . This approach allows us to approximate the mutual information between the output and intermediate features at layer ℓ without requiring network redesign for each layer, thus maintaining flexibility and scalability. To ensure dimensional compatibility between f and g , we introduce an additional linear projection layer so that $f_{\nu_{\ell}}(\mathbf{Z}_{\ell})$ outputs a d -dimensional feature.

During optimization, we freeze the parameters of the model up to the ℓ -th layer and reuse the subsequent layers, from $\ell + 1$ to L , as $f_{\nu_{\ell}}$. These layers, together with the projection layer, are randomly initialized and trained to optimize the InfoNCE objective. Both the retain and forget sets are used to provide representations for $Y = 0$ and $Y = 1$, ensuring that information from both outcomes is captured for mutual information estimation.

This approach enables $f_{\nu_{\ell}}$ to effectively exploit intermediate features \mathbf{Z}_{ℓ} to classify Y , providing deeper insights into the model’s internal information processing at each layer. It also reveals the model’s capacity to extract and utilize relevant information for distinguishing between output

labels, offering a clearer understanding of the information dynamics across the network.

4.2 Residual Information in Unlearned Models

We begin by plotting the estimated MI between the intermediate layers and the binary label indicating whether the data belong to the forget set, as shown in Figure 4b. As expected, MI decreases across layers, aligning with the Information Bottleneck principle (Tishby, Pereira, and Bialek 2000). This figure also reveals the internal behaviors of unlearned models that black-box assessments fail to capture.

In particular, SCRUB and ℓ_1 -sparse, which approximate the MI levels of Retrain, are more likely to achieve the MU objective at the feature level across both ResNet architectures. Their lower MI suggests that their encoders, like Retrain, struggle to differentiate between the forget set and the retain set. Conversely, SALUN and RL show MI curves that are close to that of Original, indicating the opposite. Note that HD produces the identical curve as Original, as its encoder remains unchanged. We observe similar patterns in CIFAR-100 and ImageNet-1K, as well as in ViT. Additionally, extending our experiment to multi-class forgetting tasks (e.g., 20 classes on CIFAR-100) reveals more pronounced MI differences between Retrain and Original. See Section E.1 for further results.

4.3 Information Difference Index (IDI)

Motivated from the above experiment, we define the **information difference (ID)** of $\theta_{\mathbf{u}}$ as the MI difference across intermediate layers between the unlearned model and Retrain, calculated as:

$$\text{ID}(\theta_{\mathbf{u}}) = \sum_{\ell=1}^L (I(\mathbf{Z}_{\ell}^{\mathbf{u}}; Y) - I(\mathbf{Z}_{\ell}^{\mathbf{r}}; Y)). \quad (1)$$

ID of $\theta_{\mathbf{u}}$ shows the extent of information retention through ensuing layers of the unlearned encoder. To provide a normalized measure, we introduce the **information difference index (IDI)**:

$$\text{IDI}(\theta_{\mathbf{u}}) = \frac{\text{ID}(\theta_{\mathbf{u}})}{\text{ID}(\theta_{\mathbf{0}})} = \frac{\sum_{\ell=1}^L (I(\mathbf{Z}_{\ell}^{\mathbf{u}}; Y) - I(\mathbf{Z}_{\ell}^{\mathbf{r}}; Y))}{\sum_{\ell=1}^L (I(\mathbf{Z}_{\ell}^{\mathbf{o}}; Y) - I(\mathbf{Z}_{\ell}^{\mathbf{r}}; Y))}, \quad (2)$$

where $\mathbf{Z}_{\ell}^{\mathbf{o}}$ is the output of the ℓ -th layer of Original encoder. Figure 4a illustrates IDI, which is conceptually the ratio of the areas between MI curves.

However, computing MI for all L layers can be expensive. In practice, we compute MI from the last n layers (i.e., later blocks), where $n \ll L$, as earlier layers show negligible differences between Retrain and Original (Figure 4b). To reduce overhead, we reuse the original network structure for MI estimation (see Figure 5). With this setup, computing IDI on CIFAR-100 with ResNet-18 takes under 5 minutes. Further details and cost analysis are provided in Section E.2.

IDI quantifies the information gap between the unlearned model and Retrain. An IDI of 0 denotes that the unlearned model has completely removed all information related to the forget set, achieving indistinguishability from Retrain. In

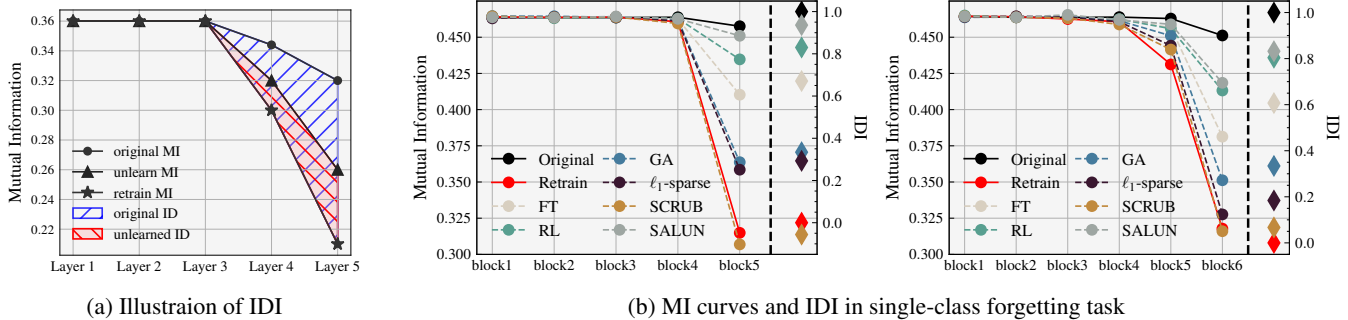


Figure 4: (a) Conceptual illustration of IDI. Curves show estimated mutual information $I(\mathbf{Z}_\ell; Y)$ for Original (●), unlearned (▲), and Retrain (★). IDI is the ratio $\frac{\text{ID}(\theta_{\text{u}})}{\text{ID}(\theta_{\text{o}})}$, corresponding to the red area divided by the blue area. (b) MI curves and IDI values for Original, Retrain, and unlearned models (FT, RL, GA, ℓ_1 -sparse, SCRUB, SALUN) on CIFAR-10 across ResNet-18 (left) and ResNet-50 (right) blocks, averaged over five trials. See Section D.2 for standard deviations.

Methods	CIFAR-10 (single class)						ImageNet-1K (five classes)					
	UA	RA	TA	MIA	IDI	RTE (min)	UA	RA	TA	MIA	IDI	RTE (min)
Retrain	100.0	100.0	95.64	10.64	0.0	154.56	100.0	88.80	75.88	9.41	0.0	2661.90
HD	100.0 ± 0.0	100.0 ± 0.0	95.22 ± 0.07	2.05 ± 0.11	1.000 ± 0.0	0.10 ± 0.01	100.0 ± 0.0	87.94 ± 0.16	<u>75.60</u> ± 0.07	7.12 ± 0.12	1.000 ± 0.0	4.75 ± 0.03
FT	100.0 ± 0.0	100.0 ± 0.0	95.12 ± 0.09	0.17 ± 0.05	0.671 ± 0.008	6.44 ± 0.07	100.0 ± 0.0	88.52 ± 0.0	<u>76.16</u> ± 0.01	8.24 ± 1.23	0.102 ± 0.026	140.04 ± 1.42
RL	99.93 ± 0.01	100.0 ± 0.0	95.66 ± 0.05	0.0 ± 0.0	0.830 ± 0.005	3.09 ± 0.03	<u>99.96</u> ± 0.03	86.46 ± 0.07	75.23 ± 0.01	0.23 ± 0.01	1.002 ± 0.007	200.73 ± 1.87
GA	100.0 ± 0.0	99.06 ± 0.25	93.10 ± 0.50	25.37 ± 3.24	0.334 ± 0.014	4.00 ± 0.08	100.0 ± 0.0	80.77 ± 0.22	71.49 ± 0.10	4.20 ± 0.46	0.328 ± 0.023	212.14 ± 2.61
Bad-T	99.90 ± 0.14	<u>99.99</u> ± 0.0	94.99 ± 0.12	68.17 ± 42.80	1.014 ± 0.004	4.64 ± 0.05	98.01 ± 0.02	84.03 ± 0.03	73.42 ± 0.03	69.13 ± 12.57	1.152 ± 0.011	211.52 ± 0.96
EU-5	100.0 ± 0.0	100.0 ± 0.0	95.25 ± 0.02	0.06 ± 0.03	0.528 ± 0.005	1.54 ± 0.0	100.0 ± 0.0	79.62 ± 0.0	71.22 ± 0.13	13.33 ± 1.53	0.183 ± 0.028	193.38 ± 0.78
CF-5	98.13 ± 1.39	100.0 ± 0.0	<u>95.54</u> ± 0.09	0.0 ± 0.0	0.675 ± 0.027	1.57 ± 0.03	100.0 ± 0.0	84.31 ± 0.08	74.16 ± 0.06	10.21 ± 5.33	0.701 ± 0.014	81.53 ± 0.56
EU-10	100.0 ± 0.0	99.50 ± 0.02	93.61 ± 0.08	15.24 ± 1.08	-0.349 ± 0.019	2.42 ± 0.11	100.0 ± 0.0	71.84 ± 0.03	65.78 ± 0.02	16.65 ± 1.91	<u>-0.051</u> ± 0.021	193.79 ± 0.47
CF-10	100.0 ± 0.0	99.98 ± 0.0	94.95 ± 0.05	11.61 ± 0.91	-0.060 ± 0.017	2.31 ± 0.03	100.0 ± 0.0	80.87 ± 0.04	72.34 ± 0.08	13.99 ± 5.41	0.608 ± 0.012	82.29 ± 0.34
SCRUB	100.0 ± 0.0	100.0 ± 0.0	95.37 ± 0.04	19.73 ± 1.92	<u>-0.056</u> ± 0.008	3.49 ± 0.02	99.28 ± 0.07	<u>88.39</u> ± 0.04	76.51 ± 0.03	7.42 ± 0.51	0.517 ± 0.011	426.04 ± 2.98
SALUN	<u>99.99</u> ± 0.01	100.0 ± 0.0	95.42 ± 0.12	0.01 ± 0.01	0.936 ± 0.012	3.54 ± 0.11	89.67 ± 0.27	86.25 ± 0.15	75.54 ± 0.10	0.50 ± 0.09	0.343 ± 0.017	793.82 ± 3.32
ℓ_1 -sparse	100.0 ± 0.0	99.93 ± 0.02	94.90 ± 0.10	1.56 ± 0.09	0.293 ± 0.012	2.96 ± 0.03	97.57 ± 0.61	85.33 ± 0.07	74.77 ± 0.03	<u>8.84</u> ± 1.39	0.239 ± 0.031	226.74 ± 1.35
COLA	100.0 ± 0.0	100.0 ± 0.0	95.36 ± 0.06	<u>12.64</u> ± 0.92	0.010 ± 0.006	4.91 ± 0.04	100.0 ± 0.0	87.93 ± 0.05	76.15 ± 0.04	9.95 ± 1.21	0.040 ± 0.042	171.44 ± 0.75

Table 1: Performance summary of MU methods (including COLA and 14 other baselines) for class-wise forgetting task on (CIFAR-10, ResNet-18) and (ImageNet-1K, ResNet-50). A better performance of an MU method corresponds to a smaller performance gap with Retrain (except RTE), with the top method in **bold** and the second best underlined.

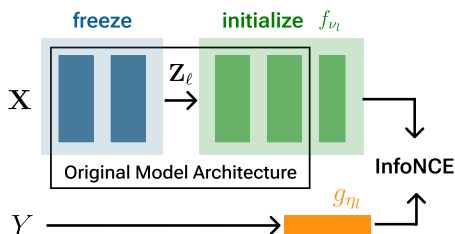


Figure 5: Illustration of estimating MI using InfoNCE. f_{v_ℓ} represents a trainable network to capture features from \mathbf{Z}_ℓ , while g_{m_ℓ} handles the binary input Y .

contrast, an IDI of 1 indicates that the encoder retains all the information found in Original. Interestingly, a negative IDI value, termed *over-unlearning*, occurs when the model removes more information than Retrain. We also demonstrate IDI for random data forgetting in Section A.1.

Note that as the denominator of IDI ($\text{ID}(\theta_o)$) approaches zero, IDI may yield unexpected values. However, this case indicates that Original and Retrain are nearly identical, suggesting minimal unlearning utility. Thus, $\text{ID}(\theta_o)$ can serve as an indicator for the necessity of unlearning in practice.

5 Experiments

5.1 COLLAPSE and ALIGN (COLA) Approach

As discussed in both Section 3 and 4.2, we observed residual information in the intermediate layers of several unlearned models, despite their outputs being similar to those of Retrain. To address this, we propose a robust two-step unlearning framework, **COLLAPSE and ALIGN (COLA)**, consisting of a *collapse phase* and an *alignment phase* to directly remove residual information at the feature level.

During the *collapse phase*, COLA eliminates feature-level information by applying supervised contrastive loss (Khosla et al. 2020) to encoder outputs. Rather than dispersing features from the forget set, which could harm model performance, COLA applies the loss to the retain set, promoting tight intra-class clustering. As these clusters shrink, features from the forget set are forced to collapse into the clusters of the retain set, achieving catastrophic forgetting. After feature collapsing, the *alignment phase* optimizes the entire model using cross-entropy loss on the retain set to align the encoder and head. For an illustration of COLA, as well as COLA+, a method tailored for random data forgetting, and detailed loss formulations, refer to Section C.7.

5.2 Evaluation of Unlearning Methods with IDI

We demonstrate the utility of IDI as a valuable efficacy metric and highlight the strong performance of COLA and its variant COLA+ through extensive experiments. Our experiments cover three datasets: CIFAR-10, CIFAR-100 (Krizhevsky 2009), and ImageNet-1K (Deng et al. 2009), and three model architectures: ResNet-18, ResNet-50 (He et al. 2016), and ViT (Dosovitskiy et al. 2021). For simplicity, we approximate IDI using the features from blocks rather than every layer in ResNet and ViT. See Section C for experimental details.

Methods	CIFAR-10 (500 samples per class)						
	UA	RA	TA	MIA	JSD	IDI	RTE (min)
Retrain	3.94	100.0	95.26	75.12	0.0	0.0	152.87
HD	<u>3.64</u> ± 1.66	97.93 ± 1.38	92.80 ± 1.18	<u>77.47</u> ± 4.09	0.08 ± 0.04	1.000 ± 0.0	0.30 ± 0.05
FT	5.03 ± 0.40	98.95 ± 0.21	92.94 ± 0.26	83.52 ± 0.58	0.07 ± 0.11	<u>-0.069</u> ± 0.013	8.11 ± 0.03
RL	4.77 ± 0.27	99.92 ± 0.0	93.54 ± 0.04	22.47 ± 1.19	0.38 ± 0.02	0.084 ± 0.030	2.75 ± 0.01
GA	2.86 ± 0.76	98.37 ± 0.71	91.90 ± 0.70	85.49 ± 2.17	0.09 ± 0.01	0.924 ± 0.028	4.31 ± 0.03
Bad-T	5.47 ± 1.05	<u>99.87</u> ± 0.05	91.51 ± 0.61	39.53 ± 3.43	0.27 ± 0.03	0.939 ± 0.053	4.78 ± 0.09
EU-10	3.16 ± 0.19	98.68 ± 0.08	93.07 ± 0.12	83.40 ± 0.21	<u>0.06</u> ± 0.01	-0.110 ± 0.013	2.13 ± 0.05
CF-10	2.71 ± 0.24	99.11 ± 0.06	<u>93.47</u> ± 0.15	84.33 ± 0.05	0.05 ± 0.01	0.219 ± 0.029	<u>2.10</u> ± 0.06
SCRUB	4.31 ± 1.50	96.21 ± 1.70	88.83 ± 1.86	37.88 ± 7.65	0.56 ± 0.09	0.322 ± 0.016	3.37 ± 0.05
SALUN	2.74 ± 0.30	97.77 ± 0.04	91.68 ± 0.44	83.52 ± 2.20	0.10 ± 0.03	0.861 ± 0.012	5.69 ± 0.04
ℓ_1 -sparse	5.47 ± 0.22	96.66 ± 0.07	91.31 ± 0.25	77.12 ± 0.21	0.09 ± 0.01	-0.157 ± 0.026	3.03 ± 0.04
COLA+	3.90 ± 0.08	99.24 ± 0.17	93.23 ± 0.09	83.48 ± 0.10	<u>0.06</u> ± 0.01	0.024 ± 0.010	7.80 ± 0.02

Table 2: Performance summary for random data forgetting on (CIFAR-10, ResNet-18), with the top method in **bold** and the second best underlined.

Table 1 shows the experimental results on CIFAR-10 and ImageNet-1K in class-forgetting tasks. At first glance, excluding the IDI column, several methods show similar accuracy (UA, RA, TA) but greater deviations in efficacy (MIA) and efficiency (RTE). This suggests that previous unlearning studies likely ranked MU methods based on MIA and RTE. However, as discussed earlier, relying solely on black-box metrics can be misleading, as they fail to account for residual information. Indeed, some methods show strong MIA performance but fail to remove forget data from intermediate layers, as reflected by high IDI values. For instance, CF-5 on ImageNet-1K achieves a favorable MIA value (10.21) close to Retrain (9.41) in the shortest time (81.53 min), yet its IDI (0.701) shows significant retention of forget data. Similarly, EU-5 on CIFAR-10, which appears highly efficient (1.54 min), presents a high IDI (0.528), suggesting that its efficiency stems from incomplete unlearning. The discrepancy between black-box metrics (MIA, JSD) and IDI is similarly observed in random data forgetting, as shown in Table 2, particularly for methods like SALUN. By incorporating IDI alongside existing metrics, we gain a more comprehensive and insightful evaluation of MU methods.

5.3 Discussions

IDI as a Real-World Efficacy Metric. Accuracy metrics (UA, RA, TA) and efficacy metrics (MIA, JSD), commonly used in recent unlearning studies, require the presence of Retrain as a gold standard to compare model outputs. While this approach is crucial for advancing MU methods in controlled experimental settings, where the field of unlearning for DNNs is still in its infancy, it becomes impractical in real-world applications where Retrain is unavailable. Similar to current black-box metrics, the original formulation of

IDI (see Equations 1 and 2) uses Retrain as a reference to assess unlearning efficacy. However, IDI allows for flexibility by using any available unlearned model as the reference. Although the absence of Retrain changes the interpretation of IDI (*i.e.*, an IDI of zero means complete unlearning as Retrain), it still provides valuable insights relative to the chosen reference. This adaptability enhances the IDI’s practicality, making it useful for evaluating unlearned models even in real-world scenarios. A detailed explanation and examples are provided in Section E.3.

Methods	CIFAR-10			CIFAR-100		
	Activation	Gradient	IDI	Activation	Gradient	IDI
Original	99.98 ± 0.03	100.0 ± 0.0	1.000	53.13 ± 2.88	61.34 ± 3.23	1.000
Retrain	94.89 ± 1.07	95.13 ± 1.12	0.000	52.87 ± 6.15	59.12 ± 4.12	0.000
Random	52.89 ± 41.03	45.23 ± 23.04	-1.281 ± 0.018	53.20 ± 5.15	47.12 ± 7.21	-2.955 ± 0.046
RL	100.0 ± 0.0	99.98 ± 0.01	0.830 ± 0.005	93.20 ± 3.53	95.30 ± 0.82	0.467 ± 0.010
GA	97.07 ± 0.35	96.01 ± 0.13	0.334 ± 0.014	97.44 ± 2.12	82.44 ± 0.95	0.392 ± 0.021
EU-10	86.13 ± 4.78	89.42 ± 2.32	-0.349 ± 0.019	64.41 ± 1.65	72.13 ± 4.13	-0.221 ± 0.009
CF-10	97.99 ± 0.38	98.33 ± 0.23	-0.060 ± 0.017	21.62 ± 0.61	23.15 ± 1.23	0.175 ± 0.040
SCRUB	99.43 ± 0.09	99.15 ± 0.05	-0.056 ± 0.008	46.44 ± 1.28	62.31 ± 1.73	0.339 ± 0.069
COLA	92.26 ± 0.08	93.12 ± 0.11	0.010 ± 0.006	61.08 ± 0.23	65.24 ± 0.43	-0.037 ± 0.006

Table 3: Performance of MU methods on white-box MIAs (Activation, Gradient) and IDI for single-class forgetting on ResNet-18. MIA values represent the attack success rate (%) for distinguishing forgetting samples. “Random” refers to a model randomly initialized without prior training.

IDI compare to White-Box MIA. While black-box MIA, adapted from privacy studies, is widely used as an evaluation tool in unlearning literature, we explore the potential of white-box MIA, which has not traditionally been employed for this purpose, and compare it with IDI. Specifically, we evaluate two white-box MIA methods: one leveraging model activations and another utilizing gradients (Nasr, Shokri, and Houmansadr 2019). Table 3 presents the results of white-box MIA and IDI in single-class forgetting scenarios. White-box MIA delivers consistent results on CIFAR-10 but becomes unstable as the dataset scales to CIFAR-100, with significant variability in MIA values across algorithms. This instability is further highlighted with a randomly initialized model, which produces MIA values comparable to Retrain despite no actual training. In contrast, IDI provides stable and interpretable results, yielding strongly negative values for randomly initialized models, accurately reflecting their lack of residual information. This underscores IDI’s reliability as a robust and interpretable metric for unlearning evaluation.

6 Conclusion

Black-box metrics often overlook critical intermediate features, limiting their effectiveness in assessing unlearning. To address this, we propose the Information Difference Index (IDI), a practical white-box metric that quantifies residual information in model features. Our experiments confirm IDI’s effectiveness for robust unlearning assessment across diverse datasets and architectures. Additionally, we introduce COLA, a novel unlearning algorithm that collapses and realigns feature representations to eliminate residual information. By examining deep representational traces rather than just superficial outputs, our work provides a more comprehensive framework for evaluating unlearning techniques.

References

- Aldaghri, N.; Mahdaviifar, H.; and Beirami, A. 2021. Coded machine unlearning. *IEEE Access*.
- Becker, A.; and Liebig, T. 2022. Evaluating machine unlearning via epistemic uncertainty. *arXiv preprint arXiv:2208.10836*.
- Bourtoule, L.; Chandrasekaran, V.; Choquette-Choo, C. A.; Jia, H.; Travers, A.; Zhang, B.; Lie, D.; and Papernot, N. 2021. Machine unlearning. In *S&P*.
- Carlini, N.; Chien, S.; Nasr, M.; Song, S.; Terzis, A.; and Tramer, F. 2022. Membership inference attacks from first principles. In *S&P*.
- Chen, M.; Gao, W.; Liu, G.; Peng, K.; and Wang, C. 2023. Boundary unlearning: Rapid forgetting of deep networks via shifting the decision boundary. In *CVPR*.
- Chundawat, V. S.; Tarun, A. K.; Mandal, M.; and Kankanhalli, M. 2023a. Can bad teaching induce forgetting? unlearning in deep networks using an incompetent teacher. In *AAAI*.
- Chundawat, V. S.; Tarun, A. K.; Mandal, M.; and Kankanhalli, M. 2023b. Zero-shot machine unlearning. *IEEE TIFS*.
- Cotogni, M.; Bonato, J.; Sabetta, L.; Pelosin, F.; and Nicolosi, A. 2023. Duck: Distance-based unlearning via centroid kinematics. *arXiv preprint arXiv:2312.02052*.
- Deng, J.; Dong, W.; Socher, R.; Li, L.-J.; Li, K.; and Fei-Fei, L. 2009. Imagenet: A large-scale hierarchical image database. In *CVPR*.
- Dosovitskiy, A.; Beyer, L.; Kolesnikov, A.; Weissenborn, D.; Zhai, X.; Unterthiner, T.; Dehghani, M.; Minderer, M.; Heigold, G.; Gelly, S.; et al. 2021. An image is worth 16x16 words: Transformers for image recognition at scale. *ICLR*.
- Dwork, C.; and Roth, A. 2014. The Algorithmic Foundations of Differential Privacy. *Found. Trends Theor. Comput. Sci.*
- Fan, C.; Liu, J.; Zhang, Y.; Wei, D.; Wong, E.; and Liu, S. 2024. Salun: Empowering machine unlearning via gradient-based weight saliency in both image classification and generation. In *ICLR*.
- Foster, J.; Schoepf, S.; and Brintrup, A. 2024. Fast machine unlearning without retraining through selective synaptic dampening. In *AAAI*.
- French, R. M. 1999. Catastrophic forgetting in connectionist networks. *Trends Cogn Sci.*
- Goel, S.; Prabhu, A.; Sanyal, A.; Lim, S.-N.; Torr, P.; and Kumaraguru, P. 2022. Towards adversarial evaluations for inexact machine unlearning. *arXiv preprint arXiv:2201.06640*.
- Golatkar, A.; Achille, A.; and Soatto, S. 2020. Eternal sunshine of the spotless net: Selective forgetting in deep networks. In *CVPR*.
- Graves, L.; Nagisetty, V.; and Ganesh, V. 2021. Amnesiac machine learning. In *AAAI*.
- Hayes, J.; Shumailov, I.; Triantafillou, E.; Khalifa, A.; and Papernot, N. 2024. Inexact unlearning needs more careful evaluations to avoid a false sense of privacy. *arXiv preprint arXiv:2403.01218*.
- He, K.; Zhang, X.; Ren, S.; and Sun, J. 2016. Deep Residual Learning for Image Recognition. In *CVPR*.
- Hinton, G.; Vinyals, O.; and Dean, J. 2014. Distilling the knowledge in a neural network. *NIPS Workshop*.
- Jia, C.; Yang, Y.; Xia, Y.; Chen, Y.-T.; Parekh, Z.; Pham, H.; Le, Q.; Sung, Y.-H.; Li, Z.; and Duerig, T. 2021. Scaling up visual and vision-language representation learning with noisy text supervision. In *ICML*.
- Jia, J.; Liu, J.; Ram, P.; Yao, Y.; Liu, G.; Liu, Y.; Sharma, P.; and Liu, S. 2023. Model Sparsity Can Simplify Machine Unlearning. In *NeurIPS*.
- Khosla, P.; Teterwak, P.; Wang, C.; Sarna, A.; Tian, Y.; Isola, P.; Maschinot, A.; Liu, C.; and Krishnan, D. 2020. Supervised contrastive learning. In *NeurIPS*.
- Kim, H.; Lee, S.; and Woo, S. S. 2024. Layer Attack Unlearning: Fast and Accurate Machine Unlearning via Layer Level Attack and Knowledge Distillation. In *AAAI*.
- Kirichenko, P.; Izmailov, P.; and Wilson, A. G. 2023. Last layer re-training is sufficient for robustness to spurious correlations. *ICLR*.
- Kirkpatrick, J.; Pascanu, R.; Rabinowitz, N.; Veness, J.; Desjardins, G.; Rusu, A. A.; Milan, K.; Quan, J.; Ramalho, T.; Grabska-Barwinska, A.; et al. 2017. Overcoming catastrophic forgetting in neural networks. *PNAS*.
- Krizhevsky, A. 2009. Learning Multiple Layers of Features from Tiny Images.
- Kurmanji, M.; Triantafillou, P.; Hayes, J.; and Triantafillou, E. 2023. Towards unbounded machine unlearning. In *NeurIPS*.
- Mu, S.; and Klabjan, D. 2024. Rewind-to-Delete: Certified Machine Unlearning for Nonconvex Functions. *arXiv preprint arXiv:2409.09778*.
- Nasr, M.; Shokri, R.; and Houmansadr, A. 2019. Comprehensive privacy analysis of deep learning: Passive and active white-box inference attacks against centralized and federated learning. In *IEEE S&P*.
- Neel, S.; Roth, A.; and Sharifi-Malvajerdi, S. 2021. Descent-to-delete: Gradient-based methods for machine unlearning. In *ALT*.
- Nguyen, T. T.; Huynh, T. T.; Nguyen, P. L.; Liew, A. W.-C.; Yin, H.; and Nguyen, Q. V. H. 2022. A survey of machine unlearning. *arXiv preprint arXiv:2209.02299*.
- Oord, A. v. d.; Li, Y.; and Vinyals, O. 2018. Representation learning with contrastive predictive coding. *arXiv preprint arXiv:1807.03748*.
- Poole, B.; Ozair, S.; Van Den Oord, A.; Alemi, A.; and Tucker, G. 2019. On variational bounds of mutual information. In *ICML*.
- Poppi, S.; Sarto, S.; Cornia, M.; Baraldi, L.; and Cucchiara, R. 2024. Multi-Class Unlearning for Image Classification via Weight Filtering. *IEEE Intelligent Systems*.
- Qiao, X.; Zhang, M.; Tang, M.; and Wei, E. 2024. Efficient Online Unlearning via Hessian-Free Recollection of Individual Data Statistics. *arXiv preprint arXiv:2404.01712*.

- Radford, A.; Kim, J. W.; Hallacy, C.; Ramesh, A.; Goh, G.; Agarwal, S.; Sastry, G.; Askell, A.; Mishkin, P.; Clark, J.; et al. 2021. Learning transferable visual models from natural language supervision. In *ICML*.
- Rombach, R.; Blattmann, A.; Lorenz, D.; Esser, P.; and Ommer, B. 2022. High-resolution image synthesis with latent diffusion models. In *CVPR*.
- Sekhri, A.; Acharya, J.; Kamath, G.; and Suresh, A. T. 2021. Remember what you want to forget: Algorithms for machine unlearning. *NeurIPS*.
- Shaik, T.; Tao, X.; Xie, H.; Li, L.; Zhu, X.; and Li, Q. 2023. Exploring the landscape of machine unlearning: A survey and taxonomy. *arXiv preprint arXiv:2305.06360*.
- Shannon, C. E. 1948. A mathematical theory of communication. *The Bell System Technical Journal*.
- Shokri, R.; Stronati, M.; Song, C.; and Shmatikov, V. 2017. Membership inference attacks against machine learning models. In *S&P*.
- Sommer, D. M.; Song, L.; Wagh, S.; and Mittal, P. 2022. Towards probabilistic verification of machine unlearning. *PETS*.
- Tarun, A. K.; Chundawat, V. S.; Mandal, M.; and Kankanhalli, M. 2023a. Deep regression unlearning. In *ICML*.
- Tarun, A. K.; Chundawat, V. S.; Mandal, M.; and Kankanhalli, M. 2023b. Fast yet effective machine unlearning. *IEEE Trans. Neural Netw. Learn. Syst.*
- Thudi, A.; Deza, G.; Chandrasekaran, V.; and Papernot, N. 2022. Unrolling sgd: Understanding factors influencing machine unlearning. In *EuroS&P*.
- Tishby, N.; Pereira, F. C.; and Bialek, W. 2000. The information bottleneck method. *arXiv preprint physics/0004057*.
- Tishby, N.; and Zaslavsky, N. 2015. Deep learning and the information bottleneck principle. In *IEEE ITW*.
- Touvron, H.; Lavril, T.; Izacard, G.; Martinet, X.; Lachaux, M.-A.; Lacroix, T.; Rozière, B.; Goyal, N.; Hambro, E.; Azhar, F.; et al. 2023. Llama: Open and efficient foundation language models. *arXiv preprint arXiv:2302.13971*.
- van der Maaten, L.; and Hinton, G. 2008. Visualizing Data using t-SNE. *JMLR*.
- Voigt, P.; and Von dem Bussche, A. 2017. The eu general data protection regulation (gdpr). *Springer International Publishing*.
- Wu, Y.; Dobriban, E.; and Davidson, S. 2020. Deltagrad: Rapid retraining of machine learning models. In *ICML*.
- Xu, H.; Zhu, T.; Zhang, L.; Zhou, W.; and Yu, P. 2023. Machine Unlearning: A Survey. *ACM Computing Surveys*.
- Yan, H.; Li, X.; Guo, Z.; Li, H.; Li, F.; and Lin, X. 2022. ARCANE: An Efficient Architecture for Exact Machine Unlearning. In *IJCAI*.
- Yosinski, J.; Clune, J.; Bengio, Y.; and Lipson, H. 2014. How transferable are features in deep neural networks? In *NeurIPS*.
- Zeiler, M. D.; and Fergus, R. 2014. Visualizing and Understanding Convolutional Networks. In *ECCV*.
- Zhang, B.; Chen, Z.; Shen, C.; and Li, J. 2024a. Verification of machine unlearning is fragile. *ICML*.
- Zhang, B.; Dong, Y.; Wang, T.; and Li, J. 2024b. Towards certified unlearning for deep neural networks. *ICML*.

A Random Data Forgetting

Another scenario in machine unlearning (MU) is *random data forgetting*, which involves forgetting a randomly selected subset of data across multiple classes. This differs from the *class-wise forgetting* task, which aims to forget entire data from single or multiple classes.

A.1 Information Difference Index for Random Data Forgetting

To calculate the information difference index (IDI) for class-wise forgetting, we employ a binary label Y to determine whether a sample belongs to the retain or forget set. However, this approach is inadequate for random data forgetting, where samples span multiple classes and a minor fraction of each class is targeted for forgetting. As a result, no single class is completely removed. To address this, we transform the binary label Y into a multiclass label Y_C , which reflects the ground-truth class label of each sample. Consequently, we define the IDI for random data forgetting as follows:

$$\text{IDI}_{\text{random}}(\theta_{\mathbf{u}}) = \frac{\text{ID}_{\text{random}}(\theta_{\mathbf{u}})}{\text{ID}_{\text{random}}(\theta_{\mathbf{o}})}, \quad (3)$$

where $\text{ID}_{\text{random}}(\theta_{\mathbf{u}}) = \sum_{\ell=1}^L (I(\mathbf{Z}_{\ell}^{\mathbf{u}}; Y_C) - I(\mathbf{Z}_{\ell}^{\mathbf{r}}; Y_C))$. Unlike the ID computed in a class-wise forgetting, $\text{ID}_{\text{random}}(\cdot)$ utilizes only the forget set \mathcal{D}_f . Intuitively, we expect the mutual information $I(\mathbf{Z}^{\mathbf{o}}; Y_C)$ to be higher than $I(\mathbf{Z}^{\mathbf{r}}; Y_C)$ because Original explicitly learned the relationship between the forget samples and their ground truth labels, while Retrain did not. Although the labels have transitioned from binary to multiple classes, the function $f_{\nu_{\ell}}$ remains unchanged. For $g_{\eta_{\ell}}$, it now employs the C dimension of vectors, where C represents the total number of data classes.

A.2 COLA+

The core idea behind COLA is to induce catastrophic forgetting within the model’s encoder in the collapse phase, making the influence of the forget set vanish implicitly. This approach is effective for class-wise forgetting tasks, where the forget set includes distinct classes. However, it may be less effective for random data forgetting, where the forget set and retain set samples generally share the same classes and are not easily distinguishable. To address this, we aim to explicitly remove the information of the forget set through pseudo-labeling. This variant, called COLA+, assigns the second-highest predicted label to the forget set samples before unlearning with supervised contrastive loss (Khosla et al. 2020). This pseudo-labeling effectively collapsing the forget set features into the retain set clusters of other classes, while reducing the confusion of the knowledge of the retain set. The results of the COLA+ experiment on the random data forgetting task are presented in Appendix D.5.

B Network Parametrizations for InfoNCE

This section provides a detailed explanation of the parametrization of the neural network critic functions used in the InfoNCE loss, including layer-specific adaptations.

B.1 Critic Functions for InfoNCE Loss

To compute the InfoNCE loss, we parameterize two critic functions: f_{ν} and g_{η} , where ν and η represent the learnable parameters of their respective neural networks. For each layer ℓ in the network, these functions are defined as follows:

1. Critic $f_{\nu_{\ell}}$:

- $f_{\nu_{\ell}} : \mathcal{Z}_{\ell} \rightarrow \mathbb{R}^d$, where \mathcal{Z}_{ℓ} represents the feature space at layer ℓ .
- This function maps raw or intermediate features \mathbf{Z}_{ℓ} to a d -dimensional embedding space. In earlier layers, $f_{\nu_{\ell}}$ must process raw, less interpretable features, making it more complex. For later layers, where features are more structured, $f_{\nu_{\ell}}$ can leverage the refined representations for better alignment with Y .

2. Critic $g_{\eta_{\ell}}$:

- $g_{\eta_{\ell}} : \{0, 1\} \rightarrow \mathbb{R}^d$.
- For the binary variable Y , $g_{\eta_{\ell}}$ is parameterized as a pair of trainable d -dimensional vectors: $g_{\eta_{\ell}}(0)$ and $g_{\eta_{\ell}}(1)$. Depending on the label Y , the corresponding vector is selected to represent the target embedding for contrastive learning.

B.2 Layer-Specific Parameterization

Each layer ℓ has independent sets of parameters ν_{ℓ} and η_{ℓ} . This design allows the model to adapt to the varying complexity of feature representations across the network. Specifically:

- In earlier layers, $f_{\nu_{\ell}}$ focuses on extracting information from raw features \mathbf{Z}_{ℓ} , which are less structured and more challenging to interpret.
- In later layers, $f_{\nu_{\ell}}$ benefits from more refined features, enabling a more direct alignment with Y .

C Experiment Details

C.1 Detailed explanation for Head Distillation

Head Distillation (HD) employs logit distillation from the original model $\theta_{\mathbf{o}}$ for efficient machine unlearning. The unlearned model $\theta_{\mathbf{u}}$ is initialized from $\theta_{\mathbf{o}}$ with the encoder frozen and only the head remaining trainable. During the unlearning process, the head is finetuned on training dataset \mathcal{D} using KL-divergence loss to follow the masked output from $\theta_{\mathbf{o}}$, where the logit for the forgetting class is set to negative infinity while preserving the logits for the remaining classes. The illustration of HD is shown in Figure 6. This enables $\theta_{\mathbf{u}}$ to mimic a pseudo-retrained model, as the masked logits closely resemble those of Retrain.

In random data forgetting scenarios where forget samples can come from any class, we modify the HD approach while maintaining its core principle of modifying only the last layer. Instead of using logit masking, we apply gradient descent on the retain set and gradient ascent on the forget set while training only the model’s head. Our experimental results demonstrate that HD achieves strong performance on black-box metrics (accuracy, MIA, and JSD) within seconds, successfully deceiving these metrics while maintaining computational efficiency (Figures 8 to 11).

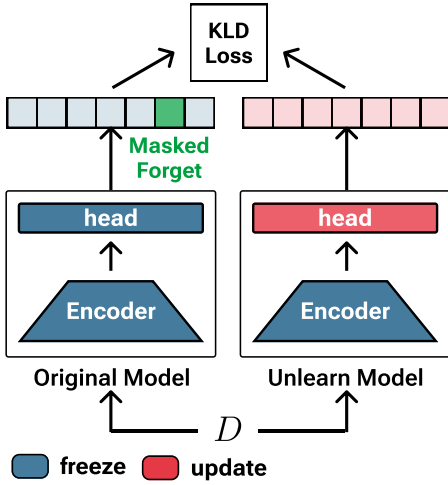


Figure 6: Overview of head distillation (HD): Original distills knowledge into the unlearn model’s head by masking the forgetting class logit, with the encoder kept frozen.

C.2 Evaluation Metrics Detail

UA, RA, TA We compute accuracy as follows:

$$\text{Acc}_{\mathcal{D}}(\theta) = \frac{1}{|\mathcal{D}|} \sum_{(x,y) \in \mathcal{D}} \mathbf{1}[\arg \max(f(x; \theta)) = y], \quad (4)$$

where $f(x; \theta)$ represents the model’s output logits for input x with parameters θ , and y is the ground truth label. Unlearning accuracy (UA), which quantifies the model’s task performance on forgetting data, is defined as $UA(\theta_u) = 1 - \text{Acc}_{\mathcal{D}_f}(\theta_u)$. Remaining accuracy (RA) measures the model’s performance on the retain set \mathcal{D}_r , which should be preserved after unlearning, and is defined as $RA(\theta_u) = \text{Acc}_{\mathcal{D}_r}(\theta_u)$. Finally, testing accuracy (TA) evaluates generalization to unseen data, and is defined as $TA(\theta_u) = \text{Acc}_{\mathcal{D}_{test}}(\theta_u)$. It is important to note that better unlearning in terms of accuracy reflects a smaller performance gap between the unlearned model and Retrain, meaning that higher accuracy levels are not necessarily better. Refer to (Jia et al. 2023) for detailed explanation.

MIA. Membership Inference Attack (MIA) (Shokri et al. 2017; Carlini et al. 2022) determines whether a specific data record was part of a model’s training set by leveraging auxiliary classifiers to distinguish between training and non-training data based on the model’s output.

In the context of unlearning, membership inference attack (MIA) is primarily used as an evaluation metric, rather than representing an adversarial scenario where an attacker attempts to extract membership information from the unlearned model. Consequently, a comparable MIA success rate on the forgetting data relative to Retrain signifies a more effective unlearning algorithm. Unlike the original MIA implementation (Shokri et al. 2017), which utilizes multiple shadow models, MIA variants in the unlearning often employ a single auxiliary classifier for each unlearning method (Jia et al. 2023). A detailed comparison of these approaches can be found in (Hayes et al. 2024).

The MIA implementation in our study has two phases: the *training phase* and the *testing phase*.

During the *training phase*, we create a balanced dataset by equally sampling from the retain set (\mathcal{D}_r) and the test set, explicitly excluding the forget set (\mathcal{D}_f). We then use this balanced dataset to train the MIA predictor with two output categories (train, non-train), allowing it to differentiate between training and non-training samples.

In the *testing phase*, the trained MIA predictor is used to evaluate the efficacy of the unlearning methods. Specifically, the **MIA** metric is calculated by applying the MIA predictor to the unlearned model (θ_u) using the forget set (\mathcal{D}_f). The objective is to determine how many samples within \mathcal{D}_f are identified as training samples by the MIA predictor.

Formally, MIA is defined as:

$$\text{MIA} = 1 - \frac{\text{TN}}{|\mathcal{D}_f|} \quad (5)$$

where TN represents the number of true negatives (*i.e.*, the number of forget samples correctly predicted as non-training examples by the MIA predictor), and $|\mathcal{D}_f|$ denotes the total number of samples in the forget set. Overall, MIA leverages privacy attack mechanisms to validate the effectiveness of the unlearning process, providing a quantitative measure of how successfully the model has ‘forgotten’ specific data re-sembling Retrain.

We consider two widely adopted variants of MIA. The first variant, **C-MIA (Confidence-based MIA)**, assesses membership based on the confidence score, which is the predicted probability of the true class (Fan et al. 2024; Jia et al. 2023). The second variant, **E-MIA (Entropy-based MIA)**, infers membership by examining the entropy of the model’s outputs, calculated as $H(x) = -\sum_i \mathbf{p}_i(x) \cdot \log \mathbf{p}_i(x)$ (Chundawat et al. 2023a; Foster, Schoepf, and Brintrup 2024; Kurmanji et al. 2023). Higher entropy indicates greater uncertainty in the model’s predictions, often signaling non-training samples. We primarily report results using E-MIA due to its more pronounced differences across various baselines compared to C-MIA. It is noteworthy that our head distillation (HD) method achieves similar performance outcomes with both E-MIA and C-MIA.

U-LiRA U-LiRA is a variant of black-box membership inference attack (MIA) designed to evaluate the privacy protection of unlearning algorithms (Hayes et al. 2024). For our LiRA MIA experiments in Section D.1, we followed the U-LiRA methodology from Hayes et al. (2024), training 128 ResNet-18 models on random splits of half the CIFAR-10 training set, ensuring that each sample is included in 64 and excluded from 64 models on average. We applied the unlearning algorithm to 40 random forget sets (200 samples each) per model, resulting in 5,120 unlearned models. For evaluation, we used 2,560 shadow and 2,560 target models, focusing on class 4 samples. Testing each method required 300–500 GPU hours, highlighting the cost-intensive nature of LiRA when adopting to unlearning; additional details can be found in (Hayes et al. 2024).

JSD Jensen-Shannon divergence (JSD) is presented in Bad-T (Chundawat et al. 2023a). It measures the distance

between the output distributions of the unlearned model and Retrain. JSD is measured as follows:

$$\text{JSD}_{\mathcal{D}}(\theta_u, \theta_r) = 0.5 \cdot KL(f(x; \theta_u) \parallel m) + 0.5 \cdot KL(f(x; \theta_r) \parallel m), \quad (6)$$

where $KL(\cdot)$ is Kullback-Leibler divergence, x is data from \mathcal{D} , and $m = \frac{f(x; \theta_u) + f(x; \theta_r)}{2}$. Here, $f(x; \theta)$ represents the model’s output probability distribution for input x with parameters θ . A smaller distance means better unlearning as the unlearned model better mimics Retrain.

RTE Runtime efficiency (RTE) measures the time that an algorithm spends to complete the unlearning, where smaller RTE indicates more efficient unlearning (Fan et al. 2024; Jia et al. 2023; Foster, Schoepf, and Brintrup 2024). Since it measures the experiment wall-clock time, it has high variance depending on the experiment environment.

C.3 Approximate MU Baselines.

We conduct our experiments on several widely used or recent approximate MU baselines: Finetuning (**FT**) (Golotkar, Achille, and Soatto 2020) finetunes Original θ_o with retain set \mathcal{D}_r , inducing catastrophic forgetting (French 1999; Kirkpatrick et al. 2017) of \mathcal{D}_f . Random labeling (**RL**) (Golotkar, Achille, and Soatto 2020) involves finetuning θ_o with randomly labeled forget set \mathcal{D}_f . Gradient ascent (**GA**) (Thudi et al. 2022) trains θ_o with reverse gradient steps using \mathcal{D}_f . **Bad-T** (Chundawat et al. 2023a) uses a teacher-student framework that utilizes distillation techniques, distinguishing between beneficial and detrimental influences through good and bad teachers to refine the learning process. Catastrophic forgetting-k (**CF-k**) and exact unlearning-k (**EU-k**) (Goel et al. 2022) involve either finetuning (CF-k) or retraining (EU-k) the last k layers of the model using \mathcal{D}_r while freezing the prior layers. **SCRUB** (Kurmanji et al. 2023) employs a technique of positive distillation from θ_o using the \mathcal{D}_r , and negative distillation on the \mathcal{D}_f , which helps in selectively retaining beneficial knowledge while discarding the unwanted influences. ℓ_1 -sparse (Jia et al. 2023) enhances the model’s ability to forget by strategically inducing weight sparsity in θ_o . **SALUN** (Fan et al. 2024) finetunes the salient weights of θ_o using a method that incorporates random labeling. For all experiments, we conduct five independent runs.

C.4 Datasets and Models

We conduct image classification experiments utilizing well-established datasets and models. The datasets include CIFAR-10, CIFAR-100 (Krizhevsky 2009), and ImageNet-1K (Deng et al. 2009); and the models are ResNet-18, ResNet-50 (He et al. 2016), and Vision Transformer (ViT) (Dosovitskiy et al. 2021). CIFAR-10 and CIFAR-100 each comprise 50,000 training images distributed across 10 and 100 classes, respectively, each with an original resolution of 32 x 32 pixels. In our experiments, we resize the images in ImageNet-1K, which consists of 1,281,167 training images across 1,000 classes, to 224 x 224 pixels. Similarly, for the ViT experiments, we resize CIFAR images to 224 x 224 pixels to accommodate the architecture’s requirements.

Throughout the training process, including pretraining and unlearning phases, we employ basic data augmentation techniques such as random cropping and random horizontal flipping.

C.5 Pretraining Settings

To perform unlearning, we require two models: **Original**, trained on the entire dataset \mathcal{D} , and **Retrain**, trained on the retain set \mathcal{D}_r . Original initializes the unlearning model. After unlearning, Retrain evaluates them. Table 4 summarizes the training configurations for each dataset and model combination. We train ResNet models from scratch and initialize ViT models with ImageNet-21K pretrained weights. For training on ImageNet-1K, we follow the configurations provided by Pytorch¹.

C.6 Unlearning Settings

We aim to follow the hyperparameters provided by the original papers. However, many hyperparameters are missing since most existing works do not experiment with large-scale datasets and models. Additionally, some values from the original papers result in poor performance, likely due to different experiment settings, as most previous work performed unlearning without any data augmentation, unlike our experiments. Therefore, we conduct thorough hyperparameter searches for each baseline. Optimal hyperparameters were identified through a fine-grained search across the range $[10^{-5}, 10^{-2}]$, evaluating values at linear steps within each decade. The detailed hyperparameters of each baseline, including our method COLA and COLA+, are shown in Table 9 and Table 10. We use the same optimizer and batch size from the original papers and focus on finding the best epoch number and learning rate in terms of unlearning accuracy (UA) and testing accuracy (TA). Note that we implement gradient ascent (GA) from SCRUB (Kurmanji et al. 2023) (referred to as ‘NegGrad+’) due to its strong performance.

C.7 COLA and COLA+ Pseudo Code

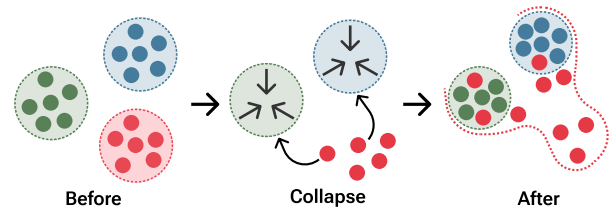


Figure 7: Illustration of the collapse phase of COLA. Features (post-encoder, pre-head) from forget set \mathcal{D}_f are represented in red, while features from retain set \mathcal{D}_r are represented in green and blue. The figure shows a class-wise forgetting task. Best viewed in color.

Algorithm 1 shows the pseudo code of our two-step framework COLA. Only using the retain set \mathcal{D}_r , in the *collapse phase* (see Figure 7), We first train the encoder of the

¹<https://github.com/pytorch/examples/tree/main/imagenet>

Settings	CIFAR-10 / CIFAR-100		ImageNet-1K	
	Resnet-18 / Resnet-50	ViT	ResNet-50	ViT
Epochs	300	3	90	30
Batch Size	128		256	512
LR	0.1	0.00002	0.1	0.02
Optimizer	SGD			
Momentum	0.9			
L2 regularization	0.0005		0	
Scheduler	CosineAnnealing			

Table 4: Training configuration for Original and Retrain.

model using supervised contrastive loss (Khosla et al. 2020) as follows:

$$\text{SupConLoss}(b, \theta_{\text{enc}}) = \frac{1}{|b|} \sum_i \frac{1}{|P(i)|} \sum_{p \in P(i)} \exp(\mathbf{z}_i \cdot \mathbf{z}_p / \tau) - \log \frac{\exp(\mathbf{z}_i \cdot \mathbf{z}_p / \tau)}{\sum_{a \in A(i)} \exp(\mathbf{z}_i \cdot \mathbf{z}_a / \tau)}, \quad (7)$$

where $P(i)$ is the set of indices of positive samples sharing the same label as sample i , $A(i)$ is the set of all indices excluding sample i , τ is a temperature, and $z_i = F(x_i; \theta_{\text{enc}})$, the output feature of the model encoder. Then we train the whole network using cross-entropy loss in the *align phase*. COLA+ additionally utilizes forget set \mathcal{D}_f in the collapse phase, where the label of forget samples is changed to the class label closest to the original label, determined by the logit output of the head of Original. Its pseudo code is presented in Algorithm 2.

C.8 IDI Details

To derive IDI from features, it is necessary to train the critic functions f_{ν_ℓ} and g_{η_ℓ} , as referenced in Section 4.1. For the training of g_{η_ℓ} , a learning rate of $5 \cdot 10^{-4}$ is applied in all architectures and datasets. Meanwhile, for f_{ν_ℓ} , the learning rates are set at $2 \cdot 10^{-5}$ for CIFAR10 ResNet-18, $2 \cdot 10^{-6}$ for ViT ImageNet-1K, and $1 \cdot 10^{-5}$ for the remaining architectures of the data set.

To get IDI, we analyzed the outputs from the layers of different models. Specifically, we evaluated the last two block outputs for ResNet18 and the final three for ResNet50. For Vision Transformer (ViT), we examined the outputs of the final three transformer encoder blocks. Note that these selections of layers is based on the observation that the information differences of outputs from the initial layers of both original and retrained models are similar. For empirical justifications of these selections, please refer to Section E.2.

C.9 System specification

For fair comparison, all experiments are executed in Python 3.10, on an Ubuntu 18.04 machine with 72 CPU cores, 4 Nvidia RTX A6000 GPUs and 512GB memory.

D Additional Unlearning Results

In this section, we provide the full experiment results on various machine unlearning settings, extending the results in Section 3 and Section 5.2.

D.1 Head Distillation (HD) Results

By achieving strong black-box performance while modifying only the model head and retaining intermediate layer information (*i.e.*, preserving the information of the forget samples), we highlighted the limitations of black-box metrics in Section 3. To examine whether HD consistently exposes these limitations across diverse metrics (e.g., Accuracy, MIA, JSD, ZRF (Chundawat et al. 2023a), AUS (Cotogni et al. 2023), LiRA MIA (Carlini et al. 2022)) and scenarios (single-class, multi-class, and random data forgetting), we extend our analysis to include a broader range of evaluations. We compare HD with five other methods: FT, RL, GA, ℓ_1 -sparse, and SALUN.

Single-Class Forgetting. Figure 8 presents the results for single-class forgetting on CIFAR-10. Despite modifying only the last layer, HD achieves the best MIA performance among the five methods. Additionally, it delivers competitive results across accuracy, JSD, ZRF, and AUS metrics, completing the task in under ten seconds (RTE). Notably, HD also performs comparably on LiRA MIA (Hayes et al. 2024), one of a recently proposed black-box MIA metrics. The strong performance of HD across various black-box metrics underscores the need for robust white-box metrics to more effectively assess unlearning quality.

Multi-Class Forgetting. For the multi-class forgetting scenario, we extend the logit masking technique of HD, as described in Section 3, by incorporating additional masking for multiple classes. As shown in Figures 9 and 10, HD achieves comparable performance across TA, MIA, JSD, ZRF, and AUS, completing the tasks within the shortest time frame (31.32 seconds for forgetting 5 classes and 25.83 seconds for forgetting 20 classes). Similar to the single-class forgetting scenario, HD’s comparable performance in this extended setup further highlights the limitations of black-box metrics.

Algorithm 1: Pseudo Code of COLA

Require: learning rate η , number of epochs E_1, E_2 , retain set $\mathcal{D}_r = \{(x_i, y_i) \mid (x_i, y_i) \in \mathcal{D}_r\}$, encoder $F(\cdot; \theta)$, and model weight $\theta = \{\theta_{\text{enc}}, \theta_{\text{head}}\}$

```

 $\theta_{\text{u,enc}} \leftarrow \theta_{\text{o,enc}}$  ▷ Collapse phase
for  $e \leftarrow 0$  to  $E_1 - 1$  do
  for all batches  $b$  of  $\mathcal{D}_r$  do
     $L = \text{SupConLoss}(b, \theta_{\text{u,enc}})$  ▷ Equation 7
     $\theta_{\text{u,enc}} \leftarrow \theta_{\text{u,enc}} - \eta \nabla_{\theta_{\text{u,enc}}} L$ 
  end for
end for

 $\theta_{\text{u,head}} \leftarrow$  random initialization ▷ Align phase
for  $e \leftarrow 0$  to  $E_2 - 1$  do
  for all batches  $b$  of  $\mathcal{D}_r$  do
     $\theta_{\text{u}} \leftarrow \theta_{\text{u}} - \eta \nabla_{\theta_{\text{u}}} L_{CE}$ 
  end for
end for
return  $\theta_{\text{u}} = \{\theta_{\text{u,enc}}, \theta_{\text{u,head}}\}$ 

```

Algorithm 2: Pseudo Code of COLA+

Require: learning rate η , number of epochs E_1, E_2 , retain set $\mathcal{D}_r = \{(x_i, y_i) \mid (x_i, y_i) \in \mathcal{D}_r\}$, forget set $\mathcal{D}_f = \{(x'_i, y'_i) \mid (x'_i, y'_i) \in \mathcal{D}_f\}$, encoder $F(\cdot; \theta)$, head $G(\cdot; \theta)$, and model weight $\theta = \{\theta_{\text{enc}}, \theta_{\text{head}}\}$

```

 $\theta_{\text{u,enc}} \leftarrow \theta_{\text{o,enc}}$  ▷ Collapse phase
 $\theta_{\text{u,head}} \leftarrow \theta_{\text{o,head}}$ 
for  $e \leftarrow 0$  to  $E_1 - 1$  do
  for  $\{b_r, b_f\}$  in all batches of  $\{\mathcal{D}_r, \mathcal{D}_f\}$  do
    for  $x'_i \in b_f$  do
       $y'_i \leftarrow \arg \max_y \text{softmax}(G(F(x'_i; \theta_{\text{u,enc}}); \theta_{\text{u,head}}))$ 
       $\mathbb{I}[y \neq y'_i]$  ▷ Pseudo-labeling
    end for
     $b \leftarrow b_r + b_f$ 
     $L = \text{SupConLoss}(b, \theta_{\text{u,enc}})$  ▷ Equation 7
     $\theta_{\text{u,enc}} \leftarrow \theta_{\text{u,enc}} - \eta \nabla_{\theta_{\text{u,enc}}} L$ 
  end for
end for ▷ Align phase

for  $e \leftarrow 0$  to  $E_2 - 1$  do
  for all batches  $b$  of  $\mathcal{D}_r$  do
     $\theta_{\text{u}} \leftarrow \theta_{\text{u}} - \eta \nabla_{\theta_{\text{u}}} L_{CE}$ 
  end for
end for
return  $\theta_{\text{u}} = \{\theta_{\text{u,enc}}, \theta_{\text{u,head}}\}$ 

```

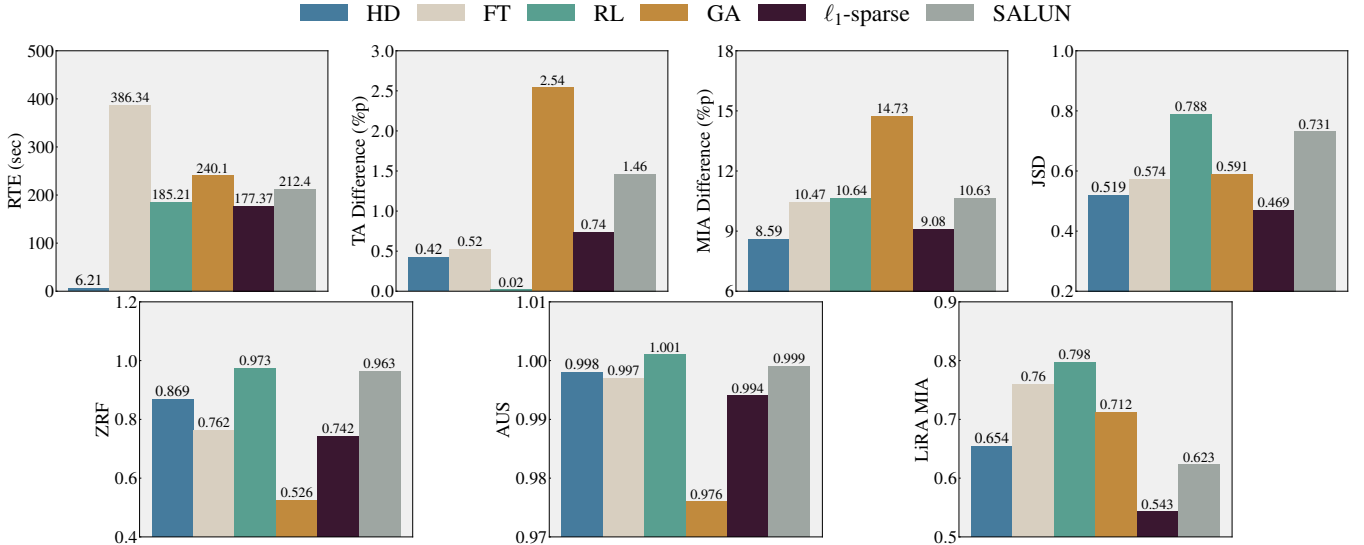


Figure 8: Performance of six methods (HD, FT, RL, GA, ℓ_1 -sparse, SALUN) on (CIFAR-10, ResNet-18), evaluated in efficiency (RTE), accuracy (TA), and efficacy (MIA, JSD, ZRF, AUS, LiRA MIA) in single-class forgetting scenarios. Lower differences from Retrain in TA, MIA, and JSD indicate closer similarity to Retrain, while higher values for ZRF and AUS represent better efficacy. Additionally, LiRA MIA values closer to 0.5 reflect higher efficacy.

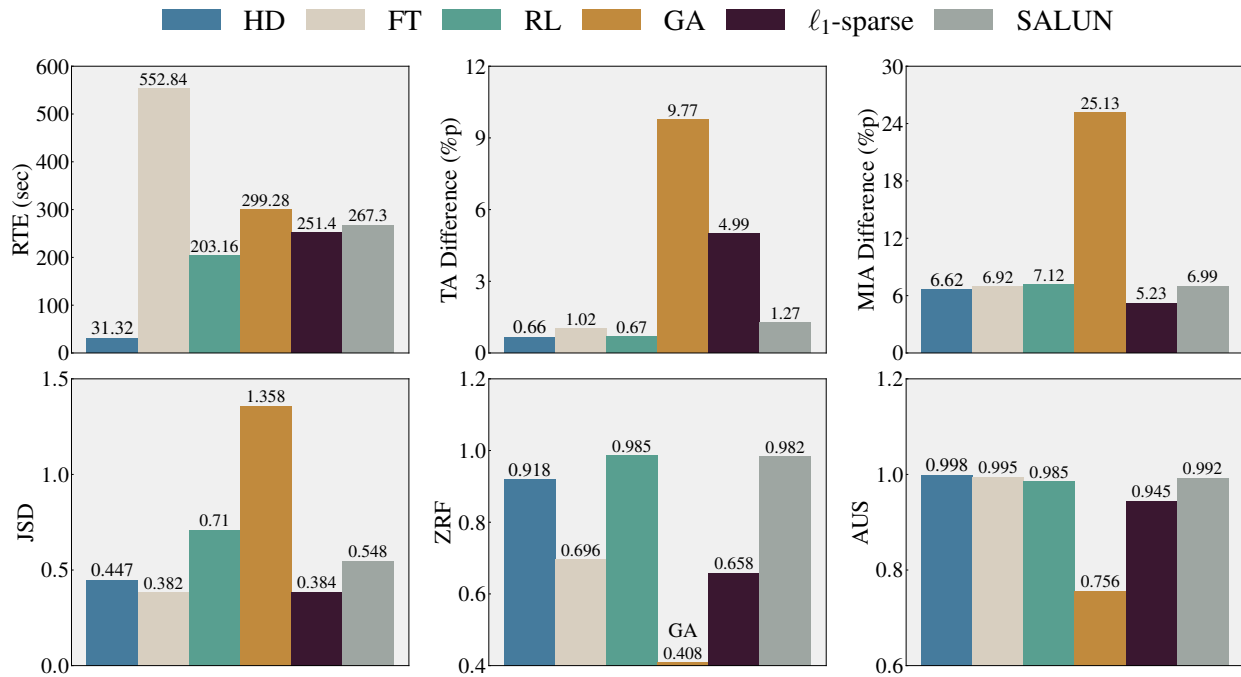


Figure 9: Performance of six methods (HD, FT, RL, GA, ℓ_1 -sparse, SALUN) on (CIFAR-100, ResNet-18), evaluated in efficiency (RTE), accuracy (TA), and efficacy (MIA, JSD, ZRF, AUS) in multi-class forgetting scenarios (5 classes). For TA, MIA, and JSD, lower differences from Retrain are preferred, indicating similarity to Retrain. For ZRF and AUS, higher values reflect better efficacy.

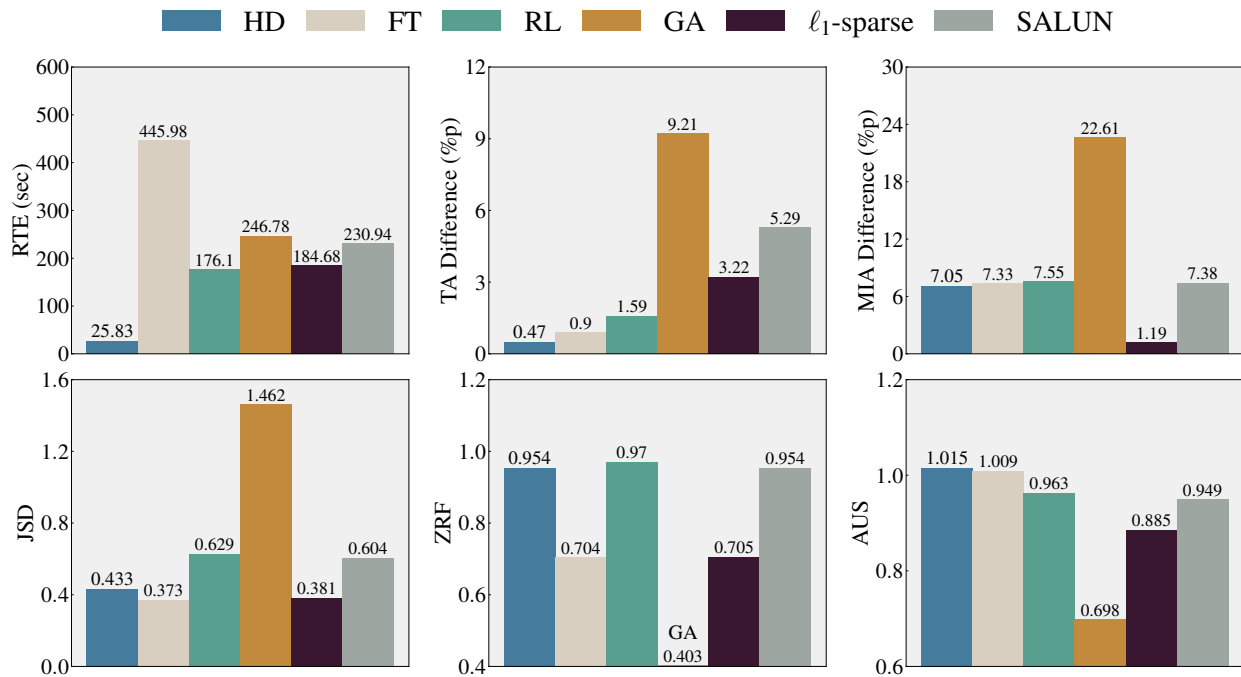


Figure 10: Performance of six methods (HD, FT, RL, GA, ℓ_1 -sparse, SALUN) on (CIFAR-100, ResNet-18), evaluated in efficiency (RTE), accuracy (TA), and efficacy (MIA, JSD, ZRF, AUS) in multi-class forgetting scenarios (20 classes). For TA, MIA, and JSD, lower differences from Retrain are preferred, indicating similarity to Retrain. For ZRF and AUS, higher values reflect better efficacy.

Random Data Forgetting. In random data forgetting scenarios, HD cannot be directly applied, as all classes are included in the retain set. To address this, we use gradient descent on the retain set and gradient ascent on the forget set while training only the model’s head. While this approach differs from HD, which uses logit masking, we retain the name to emphasize its defining characteristic of modifying only the last layer. As shown in Figure 11, HD achieves strong performance on black-box metrics (accuracy, MIA, and JSD) within less than 20 seconds (RTE). This result demonstrates that HD can still deceive black-box metrics with comparable performance. Note that ZRF is omitted in this scenario, as it is not ideally suited for random data forgetting; for more details, refer to (Chundawat et al. 2023a).

D.2 Standard Deviation

Due to the visual complexity of Figures 4 and 13, representing the standard deviation directly in these figures is challenging. Therefore, we include the standard deviation values separately in Tables 16 and 17 for Figure 4, and in Table 18 for Figure 13.

D.3 Single-Class Forgetting Results

CIFAR-10 with Various Architectures Table 11 shows the full experiment results of the single-class forgetting experiments from Table 1 on CIFAR-10 using different models. This extended table includes Jensen-Shannon divergence (JSD) and the unlearning results with ResNet-50 and ViT. Although many baselines show promising results on output based evaluation metrics, they generally exhibit poor feature-level unlearning. In contrast, COLA not only outperforms existing baselines in IDI but also shows decent results in other metrics, demonstrating its effectiveness in removing the influence of the forget set within the encoder of the model.

CIFAR-100 with Various Architectures As demonstrated in Table 12, we also compare COLA with other baselines on CIFAR-100. The results consistently highlight the difficulty of comparing and validating the efficacy of each unlearning method using existing output-based metrics. With the help of IDI, it is clear that COLA shows robustness in model unlearning on datasets with a large number of classes across various model architectures. Although SCRUB has achieved IDI near 0 for the CIFAR-10 ResNet-18 experiment, it shows significant variations in feature-level unlearning across different datasets and architectures.

D.4 Multi-Class Forgetting Results

Multi-Class Forgetting on CIFAR-10 and CIFAR-100 Table 13 presents the results of multi-class forgetting experiments on CIFAR-10 and CIFAR-100 using ResNet-18, which involves erasing the information of more than one class in the training set. We remove two classes from CIFAR-10 and five and twenty classes from CIFAR-100. Notably, many baselines exhibit higher IDI values as the number of forgetting class increases, demonstrating that the tendency to modify the head of the model strengthens with the difficulty of the unlearning tasks. In contrast, COLA

shows remarkable effectiveness, achieving metric values closely aligned with Retrain. Specifically, COLA consistently achieves the lowest IDI values among the evaluated methods, indicating the necessity of the collapse phase for effective feature-level unlearning no matter the number of class to forget.

Multi-Class Forgetting on ImageNet-1K We conduct 5-class unlearning on ImageNet-1K using ResNet-50 and ViT. Table 14 provides the complete results of Table 1 for ImageNet-1K, including all evaluation metrics and outcomes on the ViT architecture. However, it is important to note that IDI alone should not be used to assess unlearned models, as a low IDI might indicate a loss of overall information, including that from the retain set, which should be maintained at the same level as Original. This issue is evident in the RA, TA, and IDI of EU-10 and CF-10 in Table 14. In contrast, COLA consistently achieves IDI near 0 while maintaining accuracy measurements comparable to Retrain, demonstrating the scalability of our framework to the large-scale datasets.

D.5 Random Data Forgetting Results

Table 15 presents the results of the random data forgetting task conducted on ResNet-18. For CIFAR-10 and CIFAR-100 datasets, we randomly selected 500 and 50 forget samples per class, respectively. COLA+, which incorporates pseudo-labeling, successfully eliminates the influence of the forgetting data while maintaining competitive performance.

E Additional Discussions

E.1 Mutual Information Curves

Figure 17 illustrates the estimated mutual information $I(\mathbf{Z}_\ell; Y)$ of the features from the ℓ -th layer \mathbf{Z}_ℓ and the binary label Y , computed by the InfoNCE loss across various architectures and datasets. We compute mutual information (MI) for all layers from the ResNet encoder and last five layers from the ViT encoder based single-class forgetting retain and forget sets. The upper bound of MI is given by the entropy $H(Y) \geq I(\mathbf{Z}_\ell; Y) = H(Y) - H(Y | \mathbf{Z}_\ell)$. The estimated MI values fall within the range of the upper and lower bounds (0), validating the use of InfoNCE for MI estimation. Notably, all MI curves consistently show a larger difference between Original and Retrain in the later layers of the encoder across various datasets and architectures, while differences are minimal in the earlier layers. These observations underscore the validity of computing the information difference (ID) for the last few layers to quantify unlearning. Furthermore, the difference between Original and Retrain becomes more significant with increasing numbers of forget classes, as shown in Figure 18.

E.2 Effect of number of Layers for IDI

Conceptually, estimating mutual information for IDI involves all intermediate layers, as introduced in Section 4.3. However, in practice, earlier layers exhibit similar mutual information levels across models, as shown in Figure 4, Figure 17, and Figure 18. Consequently, estimating mutual in-

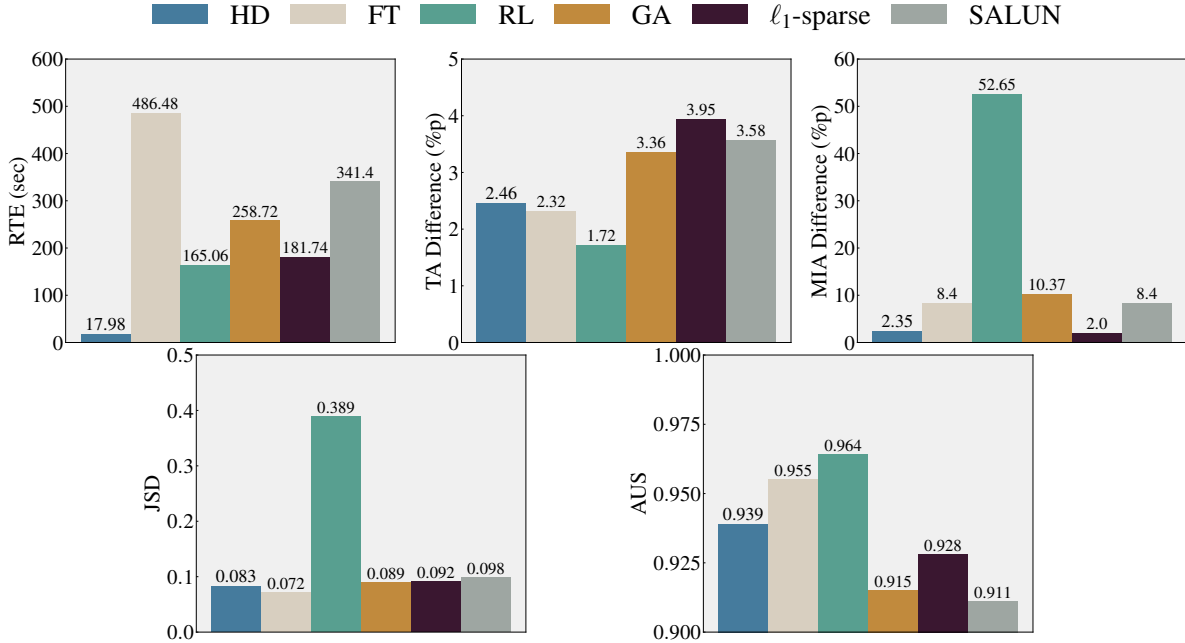


Figure 11: Performance of six methods (HD, FT, RL, GA, ℓ_1 -sparse, SALUN) on (CIFAR-10, ResNet-18), evaluated in efficiency (RTE), accuracy (TA), and efficacy (MIA, JSD, AUS) in random data forgetting scenarios (500 samples per class). For TA, MIA, and JSD, lower differences from Retrain are preferred, indicating similarity to Retrain. For AUS, higher values reflect better efficacy.

Table 5: IDI values of methods on ResNet-18 with CIFAR-10 singleclass forgetting, computed using the last n selected layers, where $n = 1$ considers only the final representation, and larger n incrementally include earlier layers. \star marks the IDI values reported in our work.

Methods	Full Layers	$n = 4$	$n = 3$	$n = 2^\star$	$n = 1$
FT	0.670 \pm 0.011	0.670 \pm 0.011	0.670 \pm 0.013	0.671 \pm 0.008	0.673 \pm 0.012
RL	0.833 \pm 0.005	0.833 \pm 0.004	0.830 \pm 0.004	0.830 \pm 0.005	0.837 \pm 0.002
GA	0.338 \pm 0.006	0.336 \pm 0.007	0.334 \pm 0.007	0.334 \pm 0.014	0.333 \pm 0.008
Bad-T	1.020 \pm 0.023	1.016 \pm 0.023	1.012 \pm 0.023	1.014 \pm 0.004	1.016 \pm 0.022
EU-5	0.531 \pm 0.004	0.531 \pm 0.005	0.530 \pm 0.006	0.528 \pm 0.005	0.524 \pm 0.007
CF-5	0.674 \pm 0.023	0.675 \pm 0.023	0.673 \pm 0.024	0.675 \pm 0.027	0.679 \pm 0.026
EU-10	-0.352 \pm 0.007	-0.347 \pm 0.007	-0.344 \pm 0.006	-0.349 \pm 0.019	-0.310 \pm 0.018
CF-10	-0.058 \pm 0.010	-0.060 \pm 0.010	-0.061 \pm 0.010	-0.060 \pm 0.017	-0.056 \pm 0.008
SCRUB	-0.055 \pm 0.028	-0.053 \pm 0.029	-0.051 \pm 0.027	-0.056 \pm 0.008	-0.048 \pm 0.026
SALUN	0.941 \pm 0.029	0.937 \pm 0.029	0.935 \pm 0.029	0.936 \pm 0.012	0.935 \pm 0.027
l1-sparse	0.292 \pm 0.011	0.293 \pm 0.012	0.294 \pm 0.011	0.293 \pm 0.012	0.297 \pm 0.013
COLA	0.010 \pm 0.009	0.012 \pm 0.009	0.012 \pm 0.008	0.010 \pm 0.006	0.015 \pm 0.013

formation from only a few later layers is sufficient for evaluation. This observation aligns with findings in Yosinski et al. (2014); Zeiler and Fergus (2014), which indicate that earlier layers primarily capture general features, while later layers focus on distinctive features, resulting in greater variability in mutual information. To validate this approach, we measure IDI using different numbers of accumulated layers from the back, as presented in Table 5 and Table 6. These experiments use the same settings discussed in Figure 4.

Our results demonstrate minimal differences in IDI as n increases, indicating a negligible contribution of earlier lay-

ers to IDI. Specifically, when comparing the two columns (“Full layers” and “ n with \star ”), the discrepancy between the ideal IDI and our practical approach is minimal, empirically supporting the validity of focusing on the last selected layers. This property is particularly beneficial for reducing computational costs, as mutual information computations for later layers require less time due to the shallower g networks involved (refer to Section 4.1). Practitioners can determine the appropriate n by observing the information gap per layer between Original and Retrain for a given unlearning setup.

Table 6: IDI values of methods on ResNet-50 with CIFAR-10 single class forgetting, computed using the last n selected layers, where $n = 1$ considers only the final representation, and larger n incrementally include earlier layers. \star marks the IDI values reported in our work.

Methods	Full Layers	$n = 5$	$n = 4$	$n = 3^\star$	$n = 2$	$n = 1$
FT	$0.617_{\pm 0.006}$	$0.618_{\pm 0.009}$	$0.618_{\pm 0.013}$	$0.607_{\pm 0.009}$	$0.610_{\pm 0.013}$	$0.563_{\pm 0.014}$
RL	$0.808_{\pm 0.012}$	$0.808_{\pm 0.012}$	$0.811_{\pm 0.006}$	$0.804_{\pm 0.006}$	$0.814_{\pm 0.003}$	$0.797_{\pm 0.000}$
GA	$0.334_{\pm 0.018}$	$0.338_{\pm 0.018}$	$0.337_{\pm 0.018}$	$0.334_{\pm 0.023}$	$0.339_{\pm 0.017}$	$0.269_{\pm 0.015}$
Bad-T	$1.156_{\pm 0.016}$	$1.151_{\pm 0.020}$	$1.152_{\pm 0.021}$	$1.153_{\pm 0.026}$	$1.157_{\pm 0.018}$	$1.163_{\pm 0.024}$
EU-5	$1.044_{\pm 0.009}$	$1.043_{\pm 0.008}$	$1.050_{\pm 0.005}$	$1.047_{\pm 0.005}$	$1.061_{\pm 0.002}$	$1.080_{\pm 0.002}$
CF-5	$0.904_{\pm 0.005}$	$0.906_{\pm 0.005}$	$0.910_{\pm 0.006}$	$0.906_{\pm 0.002}$	$0.916_{\pm 0.001}$	$0.914_{\pm 0.002}$
EU-10	$0.760_{\pm 0.014}$	$0.766_{\pm 0.011}$	$0.766_{\pm 0.011}$	$0.757_{\pm 0.011}$	$0.756_{\pm 0.010}$	$0.715_{\pm 0.010}$
CF-10	$0.592_{\pm 0.015}$	$0.594_{\pm 0.017}$	$0.590_{\pm 0.018}$	$0.579_{\pm 0.009}$	$0.582_{\pm 0.018}$	$0.516_{\pm 0.024}$
SCRUB	$0.067_{\pm 0.005}$	$0.073_{\pm 0.007}$	$0.071_{\pm 0.007}$	$0.067_{\pm 0.020}$	$0.076_{\pm 0.008}$	$0.011_{\pm 0.005}$
SALUN	$0.831_{\pm 0.014}$	$0.833_{\pm 0.011}$	$0.832_{\pm 0.019}$	$0.832_{\pm 0.027}$	$0.842_{\pm 0.009}$	$0.771_{\pm 0.005}$
ℓ_1 -sparse	$0.185_{\pm 0.005}$	$0.183_{\pm 0.007}$	$0.181_{\pm 0.007}$	$0.184_{\pm 0.023}$	$0.185_{\pm 0.016}$	$0.191_{\pm 0.007}$
COLA	$0.019_{\pm 0.006}$	$0.023_{\pm 0.009}$	$0.021_{\pm 0.009}$	$0.019_{\pm 0.025}$	$0.022_{\pm 0.009}$	$0.007_{\pm 0.011}$

Methods	CIFAR-10				CIFAR-100					
	Order	$\theta_s = \text{Retrain}$	$\theta_s = \text{COLA}$	$\theta_s = \text{EU-10}$	$\theta_s = \text{FT}^\star$	Order	$\theta_s = \text{Retrain}$	$\theta_s = \text{COLA}$	$\theta_s = \text{EU-10}$	$\theta_s = \text{FT}^\star$
FT	8	$0.671_{\pm 0.008}$	$0.668_{\pm 0.008}$	$0.756_{\pm 0.006}$	$0.662_{\pm 0.008}$	11	$0.610_{\pm 0.022}$	$0.624_{\pm 0.021}$	$0.680_{\pm 0.018}$	$0.481_{\pm 0.029}$
RL	10	$0.830_{\pm 0.005}$	$0.828_{\pm 0.005}$	$0.874_{\pm 0.004}$	$0.825_{\pm 0.005}$	9	$0.467_{\pm 0.010}$	$0.486_{\pm 0.010}$	$0.563_{\pm 0.008}$	$0.291_{\pm 0.013}$
GA	6	$0.334_{\pm 0.014}$	$0.328_{\pm 0.014}$	$0.506_{\pm 0.010}$	$0.315_{\pm 0.014}$	8	$0.392_{\pm 0.021}$	$0.414_{\pm 0.020}$	$0.502_{\pm 0.017}$	$0.191_{\pm 0.028}$
Bad-T	12	$1.014_{\pm 0.004}$	$1.014_{\pm 0.004}$	$1.010_{\pm 0.003}$	$1.014_{\pm 0.004}$	12	$1.079_{\pm 0.024}$	$1.076_{\pm 0.023}$	$1.065_{\pm 0.020}$	$1.105_{\pm 0.032}$
EU-5	7	$0.528_{\pm 0.005}$	$0.523_{\pm 0.005}$	$0.650_{\pm 0.004}$	$0.515_{\pm 0.005}$	3	$0.064_{\pm 0.037}$	$0.098_{\pm 0.036}$	$0.233_{\pm 0.030}$	$-0.245_{\pm 0.049}$
CF-5	9	$0.675_{\pm 0.027}$	$0.672_{\pm 0.027}$	$0.759_{\pm 0.020}$	$0.666_{\pm 0.028}$	7	$0.388_{\pm 0.010}$	$0.410_{\pm 0.010}$	$0.499_{\pm 0.008}$	$0.186_{\pm 0.013}$
EU-10	1	$-0.349_{\pm 0.019}$	$-0.362_{\pm 0.019}$	$0.0_{\pm 0.014}$	$-0.387_{\pm 0.020}$	1	$-0.221_{\pm 0.009}$	$-0.177_{\pm 0.009}$	$0.0_{\pm 0.007}$	$-0.624_{\pm 0.012}$
CF-10	2	$-0.060_{\pm 0.017}$	$-0.070_{\pm 0.017}$	$0.214_{\pm 0.013}$	$-0.090_{\pm 0.017}$	4	$0.175_{\pm 0.040}$	$0.205_{\pm 0.039}$	$0.324_{\pm 0.033}$	$-0.097_{\pm 0.053}$
SCRUB	3	$-0.056_{\pm 0.008}$	$-0.066_{\pm 0.008}$	$0.217_{\pm 0.006}$	$-0.086_{\pm 0.008}$	6	$0.339_{\pm 0.069}$	$0.363_{\pm 0.067}$	$0.458_{\pm 0.057}$	$0.121_{\pm 0.092}$
SALUN	11	$0.936_{\pm 0.012}$	$0.935_{\pm 0.012}$	$0.953_{\pm 0.009}$	$0.934_{\pm 0.012}$	10	$0.529_{\pm 0.022}$	$0.546_{\pm 0.021}$	$0.614_{\pm 0.018}$	$0.373_{\pm 0.029}$
ℓ_1 -sparse	5	$0.293_{\pm 0.012}$	$0.286_{\pm 0.012}$	$0.476_{\pm 0.009}$	$0.273_{\pm 0.012}$	5	$0.334_{\pm 0.026}$	$0.358_{\pm 0.025}$	$0.454_{\pm 0.021}$	$0.114_{\pm 0.035}$
COLA	4	$0.010_{\pm 0.006}$	$0.0_{\pm 0.006}$	$0.266_{\pm 0.004}$	$-0.018_{\pm 0.006}$	2	$-0.038_{\pm 0.006}$	$0.0_{\pm 0.006}$	$0.150_{\pm 0.005}$	$-0.381_{\pm 0.008}$

Table 7: IDI for four different reference models (Retrain, COLA, EU-10, and FT *). FT * is finetuned with a learning rate of $5e-5$, while FT is finetuned with a learning rate of $1e-5$. Since FT typically does not remove all residual information while maintaining test accuracy, using a higher learning rate for FT * can be justified if you want to use it as the reference model. The ‘Order’ has been arranged in ascending sequence according to the IDI values.

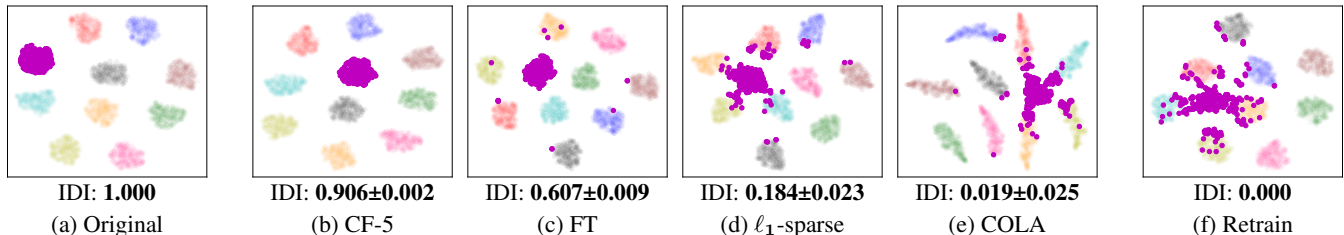


Figure 12: t-SNE visualizations of encoder outputs for Original, Retrain, and unlearned models from four MU methods (SALUN, ℓ_1 -sparse, SCRUB, EU-10) on single-class forgetting with (CIFAR-10, ResNet-50). In each t-SNE plot, features of the forgetting class are represented in purple.

E.3 IDI without Retrain Model

In real-world applications, using the Retrain is often infeasible. In such cases, any reasonable model can be used as the **standard model**, denoted as θ_s . Although the absence of a Retrain inevitably affects how the IDI value is interpreted (*i.e.*, an IDI value of zero indicates that unlearning has been properly achieved, equivalent to the Retrain), it still provides

useful insights into the degree of unlearning achieved relative to the chosen reference. To accommodate this, we introduce an extended version of the ID metric. Differences are highlighted with (\cdot) :

$$\mathbf{ID}(\theta_u, \theta_s) = \sum_{\ell=1}^L \left(I(\mathbf{Z}_\ell^{(u)}; Y_C) - I(\mathbf{Z}_\ell^{(s)}; Y_C) \right). \quad (8)$$

The main difference from the original IDI is that θ_s can be set as any model including θ_r (Retrain), while the previous version fixed $\theta_s = \theta_r$. This extension also leads to the modified IDI metric:

$$\begin{aligned} \text{IDI}(\theta_u, \theta_s) &= \frac{\text{ID}(\theta_u, \theta_s)}{\text{ID}(\theta_o, \theta_s)} \\ &= \frac{\sum_{\ell=1}^L \left(I(\mathbf{Z}_\ell^{(u)}; Y) - I(\mathbf{Z}_\ell^{(s)}; Y) \right)}{\sum_{\ell=1}^L \left(I(\mathbf{Z}_\ell^{(o)}; Y) - I(\mathbf{Z}_\ell^{(s)}; Y) \right)}. \end{aligned} \quad (9)$$

We test IDI using different reference models, as demonstrated in Table 7. Intuitively, since only the standard model changes in Equation (9), the order of the IDI values remains consistent.

E.4 IDI and t-SNE Relationship

In Section 3.2, we identified significant residual information in unlearned models through their tightly clustered t-SNE plots (see Figure 2) and their ability to easily recover forgotten information (see Figure 3). Black-box assessments failed to detect these residuals, as shown by the success of HD (see Figure 1), which only altered the last layer. In contrast, IDI effectively captures these hidden residuals, showing a strong correlation with t-SNE plots (see Figure 12), and aligning with accuracy recovered across unlearned models (see Figure 3). By complementing existing metrics, IDI offers a comprehensive evaluation of approximate MU methods, addressing crucial aspects to ensure strong unlearning beyond superficial modifications.

Figure 14 presents the full t-SNE plots illustrating the intermediate features and corresponding IDI measurements of MU baselines on the single-class unlearning on CIFAR-10 with ResNet-18. A high IDI corresponds to better clustering and similarity among features of the forgetting class, as seen in (l) SALUN and (f) Bad-T, which show inadequate unlearning performance. These examinations show the high relationship between IDI and the residual information of forget set. Additionally, the IDI metric reveals instances of over-unlearning, where the forgetting class becomes excessively dispersed, as demonstrated in (i) EU-10. Among the evaluated methods, (n) COLA has the closest IDI to Retrain, suggesting its high efficacy in achieving the desired removal of the forget set influence in the intermediate layers of the model. This trend is also visible in ResNet-50 (see Figure 15) and ViT (see Figure 16).

Furthermore, we confirm that IDI for the random data forgetting correctly captures the encoder’s information, similar to IDI for the class-wise forgetting. In Figure 20, the t-SNE plots of forget sample features for two baselines with the same unlearning accuracy (UA) – Bad-T and ℓ_1 -sparse – and their IDI values in the random data forgetting task is visualized. Comparing them, IDI successfully reflects the residual information in the features, as the features of Bad-T form more compact clusters than those of ℓ_1 -sparse, indicating more influence of the forget set remains in Bad-T. IDI for random data forgetting captures the hidden information that cannot be noticed from existing metrics, which may suggest

that both methods unlearn similarly due to their same forget accuracy.

E.5 Mutual Information and Accuracy

We extend the experiment to measure the accuracy of the intermediate features of the model’s encoder. Similar to measuring MI using the InfoNCE loss, we freeze the layers up to the ℓ -th layer of the encoder and train the remaining encoder layers and an additional head using cross-entropy loss. The additional head perform binary classification to determine whether the input belongs to the retain or forget set.

Figure 19 shows the train accuracy curves on the CIFAR-10 single-class forgetting dataset with ResNet-18. For Original encoder, the trained model readily classifies the retain and forget sets. However, for Retrain encoder, the model fails to classifies all samples at the last two layers, with the accuracy dropping more in the later layer. These curves correspond to the those from Figure 17, indicating that the estimated MI accurately reflects the model’s knowledge of the retain and forget sets. In addition, the small accuracy gap between Original and Retrain provides the necessity of MI for accurate residual information quantification.

E.6 Computational Complexity of IDI

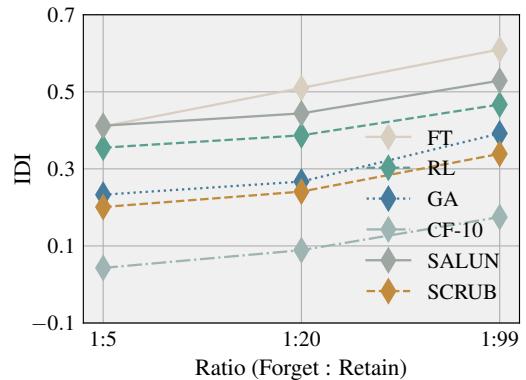


Figure 13: IDI of six methods with varying binary label ratios, in the single-class forgetting on (CIFAR-100, ResNet-18), where $a : b$ denotes the ratio of forget to retain samples.

Table 8 presents the runtime of mutual information (MI) computation for intermediate features from each block, using the MI estimation method proposed in Section 4.1, in the CIFAR-100 single-class forgetting setup with ResNet-18, ResNet-50, and ViT. Although MI estimation across all layers can be time-consuming, our selected layers for IDI computation (*i.e.*, features from the last two blocks for ResNet-18 and the last three blocks for ResNet-50 and ViT, as detailed in Section C.8, and empirically justified in Section E.2) significantly reduce runtime without harming metric performance. Specifically, the runtime decreases by factors of 2.63, 2.18, and 4.30 for ResNet-18, ResNet-50, and ViT, respectively, when the estimation is sequentially processed for each block.

Furthermore, using only 10% of the retain set improves runtime by an additional 4 to 5 times without affecting the general trend, as shown in Figure 13. Since training the latter layers requires fewer FLOPs compared to earlier layers, the

ResNet-18						ResNet-50						
Ratios	Block1	Block2	Block3	Block4	Block5	Ratios	Block1	Block2	Block3	Block4	Block5	Block6
10%	1.61 \pm 0.05	1.55 \pm 0.21	1.63 \pm 0.09	1.49 \pm 0.11	1.42 \pm 0.13	10%	4.17 \pm 0.13	3.85 \pm 0.04	3.43 \pm 0.01	3.42 \pm 0.15	3.35 \pm 0.02	3.24 \pm 0.15
Full	6.64 \pm 0.08	6.51 \pm 0.17	6.32 \pm 0.12	6.04 \pm 0.10	5.90 \pm 0.15	Full	19.91 \pm 0.18	17.70 \pm 0.01	15.75 \pm 0.02	15.32 \pm 0.11	14.98 \pm 0.07	14.83 \pm 0.04

ViT												
Ratios	Block1	Block2	Block3	Block4	Block5	Block6	Block7	Block8	Block9	Block10	Block11	Block12
10%	32.46	32.12	31.43	30.99	30.64	30.21	29.50	29.01	28.75	28.43	27.95	27.14
Full	167.00	162.81	160.64	159.56	157.65	155.35	151.82	147.78	146.05	144.25	142.81	139.61

Table 8: Runtime (in minutes) for mutual information estimation at the final layer of each block. A ‘block’ refers to a group of residual layers in ResNet (commonly referred to as stages, with four blocks in ResNet-18) or a transformer block in ViT. Results are presented for evaluations conducted using 10% of the retain set and the full dataset in the CIFAR-10 single-class forgetting scenario.

computational complexity of IDI is further reduced. These techniques can effectively alleviate potential computational challenges when applying our metric in practice.

F Broader Impact

Our work on improving machine unlearning focuses on foundational research aimed at enhancing privacy and data removal. However, there is a potential risk that our methodology could be misused to evade data retention policies or obscure accountability. Despite this possibility, it is unlikely that our work will introduce new harmful practices beyond what existing unlearning methods already permit, as we are not introducing new capabilities. Therefore, while there might be concerns related to privacy, security, and fairness, our work does not pose a greater risk compared to other foundational research in machine unlearning.

G Limitations

Our methodology accomplishes its main objective, but there are a few limitations we point out. Although our IDI successfully investigates hidden information in intermediate features, its computation requires multiple training runs, which can be computationally intensive. For instance, The computation of IDI for ResNet-50 on the CIFAR-100 dataset takes approximately 40-50 minutes. However, one can mitigate this by computing mutual information for only the last few layers, as the early stages of the encoder are largely similar for both the Retrain and Original models. Thus, this approach requires fine-tuning only the later layers, reducing the overall computational burden. Additionally, by adjusting the forget-to-retain ratio, it is possible to improve efficiency and possibly decrease the processing time to merely 3-4 minutes.

Class-wise Forgetting			
Settings	CIFAR-10 ResNet-18 / ResNet-50 / ViT	CIFAR-100 ResNet-18 / ResNet-50 / ViT	ImageNet-1K ResNet-50 / ViT
FT	25 Epochs, Adam LR $10^{-5}/10^{-5}/10^{-4}$ Retain Batch Size 64		3/4 Epochs, Adam LR 10^{-5} Retain Batch Size 128
RL	7 / 7 / 10 Epochs, SGD LR $10^{-5} / 2 \cdot 10^{-5} / 10^{-3}$ Retain Batch Size 64 Forget Batch Size 16	7 / 7 / 10 Epochs, SGD LR $2 \cdot 10^{-5} / 10^{-4} / 10^{-4}$ Retain Batch Size 64 Forget Batch Size 16	3 Epochs, SGD LR $10^{-3} / 10^{-4}$ Retain Batch Size 128 Forget Batch Size 16
GA	10 Epochs, SGD LR $2 \cdot 10^{-3} / 2 \cdot 10^{-3} / 5 \cdot 10^{-3}$ Retain Batch Size 64 Forget Batch Size 16	10 Epochs, SGD LR $9 \cdot 10^{-4} / 9 \cdot 10^{-4} / 5 \cdot 10^{-3}$ Retain Batch Size 64 Forget Batch Size 16	3 Epochs, SGD LR $2 \cdot 10^{-3} / 10^{-3}$ Retain Batch Size 128 Forget Batch Size 16
Bad-T	10 Epochs, Adam LR 10^{-5} Batch Size 256		3 Epochs, Adam LR 10^{-5} Batch Size 256
EU-5 / EU-10	14 Epochs, SGD LR 10^{-2} Retain Batch Size 64		2 Epochs, SGD LR $5 \cdot 10^{-3}$ Retain Batch Size 128
CF-5 / CF-10	14 / 14 / 18 Epochs, SGD LR $10^{-2} / 10^{-2} / 3 \cdot 10^{-2}$ Retain Batch Size 64		5 Epochs, SGD LR $5 \cdot 10^{-3}$ Retain Batch Size 128
SCRUB	3(2) Epochs, SGD LR $5 \cdot 10^{-4} / 5 \cdot 10^{-4} / 10^{-4}$ Retain Batch Size 64 Forget Batch Size 256 / 256 / 64	3(2) Epochs, SGD LR $5 \cdot 10^{-4}$ Retain Batch Size 128 Forget Batch Size 8	2(2) Epochs, SGD LR $5 \cdot 10^{-4} / 10^{-4}$ Retain Batch Size 128 Forget Batch Size 256
SALUN	10 Epochs, SGD LR $5 \cdot 10^{-4} / 10^{-3} / 10^{-3}$ Retain Batch Size 64 Forget Batch Size 16	15 Epochs, SGD LR 10^{-3} Retain Batch Size 64 Forget Batch Size 16	5/2 Epochs, SGD LR 10^{-3} Retain Batch Size 128 Forget Batch Size 16
ℓ_1 -sparse	10 Epochs, SGD LR $2 \cdot 10^{-4} / 2 \cdot 10^{-4} / 9 \cdot 10^{-4}$ Retain Batch Size 64	10 Epochs, SGD LR $2 \cdot 10^{-4} / 2 \cdot 10^{-4} / 5 \cdot 10^{-4}$ Retain Batch Size 64	5 Epochs, SGD LR $9 \cdot 10^{-4}$ Retain Batch Size 128
COLA	10+10 Epochs, Adam Contrast LR $2 \cdot 10^{-4} / 2 \cdot 10^{-4} / 1.5 \cdot 10^{-4}$ Finetune LR $5 \cdot 10^{-6} / 10^{-5} / 5 \cdot 10^{-5}$ Retain Batch Size 64	10+10 Epochs, Adam Contrast LR $5 \cdot 10^{-4} / 5 \cdot 10^{-4} / 5 \cdot 10^{-4}$ Finetune LR $5 \cdot 10^{-6} / 10^{-5} / 5 \cdot 10^{-5}$ Retain Batch Size 256	1+2 Epochs, Adam Contrast LR $2 \cdot 10^{-5} / 5 \cdot 10^{-5}$ Finetune LR $1 \cdot 10^{-5} / 5 \cdot 10^{-5}$ Retain Batch Size 256

Table 9: Hyperparameters of baselines for *class-wise forgetting*. Retain Batch Size is the batch size of retain set \mathcal{D}_r and Forget Batch Size is the batch size of forget set \mathcal{D}_f . Baselines without Forget Batch Size imply that they do not use forget set \mathcal{D}_f . Bad-T uses the entire dataset \mathcal{D} , so there is no separation of retain and forget of Batch Size. SCRUB has separate epochs for retain set and forget set, which is visualized as Retain Epochs (Forget Epochs). For COLA, A + B Epochs indicates collapse epochs A and align epochs B.

Random Data Forgetting		
Settings	CIFAR-10	CIFAR-100
	ResNet-18	
FT	25 Epochs, Adam LR 10^{-4}	LR $2 \cdot 10^{-4}$
	Retain Batch Size 64	
RL	7 Epochs, SGD LR 10^{-3}	LR $5 \cdot 10^{-4}$
	Retain Batch Size 64 Forget Batch Size 16	
GA	10 Epochs, SGD LR $2.5 \cdot 10^{-3}$	10 Epochs, SGD LR $1 \cdot 10^{-3}$
	Retain Batch Size 64 Forget Batch Size 16	
Bad-T	10 Epochs, Adam LR $1 \cdot 10^{-5}$ Batch Size 256	
EU-5 / EU-10	14 Epochs, SGD LR 10^{-1}	LR $5 \cdot 10^{-2}$
	Retain Batch Size 64	
CF-5 / CF-10	14 Epochs, SGD LR 10^{-1}	LR $5 \cdot 10^{-2}$
	Retain Batch Size 64	
SCRUB	5(5) Epochs, SGD LR $2.5 \cdot 10^{-5}$	LR $5.4 \cdot 10^{-4}$
	Retain Batch Size 16 Forget Batch Size 64	
SALUN	10 Epochs, SGD LR $8.3 \cdot 10^{-4}$	15 Epochs, SGD LR $5 \cdot 10^{-4}$
	Retain Batch Size 64 Forget Batch Size 16	
ℓ_1 -sparse	10 Epochs, SGD LR $4 \cdot 10^{-4}$	LR $3 \cdot 10^{-4}$
	Retain Batch Size 64	Retain Batch Size 64
COLA+	10+10 Epochs, Adam Contrast LR $2 \cdot 10^{-4}$ Finetune LR $1 \cdot 10^{-4}$	10+10 Epochs, Adam Contrast LR $2.5 \cdot 10^{-4}$ Finetune LR $2 \cdot 10^{-5}$
	Retain Batch Size 32 Forget Batch Size 64	Retain Batch Size 64 Forget Batch Size 192

Table 10: Hyperparameters of baselines for *random data forgetting*. Retain Batch Size is the batch size of retain set \mathcal{D}_r and Forget Batch Size is the batch size of forget set \mathcal{D}_f . Baselines without Forget Batch Size imply that they do not use forget set \mathcal{D}_f . Bad-T uses the entire dataset \mathcal{D} , so there is no separation of retain and forget of Batch Size. SCRUB uses separate epochs for retain set and forget set, which is visualized as Retain Epochs (Forget Epochs). For COLA+, A + B Epochs indicates collapse epochs A and align epochs B.

CIFAR-10 - ResNet-18							
Methods	UA	RA	TA	MIA	JSD	IDI	RTE (min)
Original	0.0	100.0	95.46	91.50	3.21	1.000	170.32
Retrain	100.0	100.0	95.64	10.64	0.0	0.0	154.56
FT	100.0 ± 0.0	100.0 ± 0.0	95.12 ± 0.09	0.17 ± 0.05	0.57 ± 0.03	0.671 ± 0.008	6.44 ± 0.07
RL	99.93 ± 0.01	100.0 ± 0.0	95.66 ± 0.09	0.0 ± 0.0	0.79 ± 0.01	0.830 ± 0.005	3.09 ± 0.03
GA	100.0 ± 0.0	99.06 ± 0.25	93.10 ± 0.50	25.37 ± 3.24	0.59 ± 0.05	0.334 ± 0.014	4.00 ± 0.08
Bad-T	99.90 ± 0.14	<u>99.99</u> ± 0.0	94.99 ± 0.12	68.17 ± 42.80	3.69 ± 0.85	1.014 ± 0.004	4.64 ± 0.05
EU-5	100.0 ± 0.0	100.0 ± 0.0	95.25 ± 0.02	0.06 ± 0.03	0.53 ± 0.02	0.528 ± 0.005	1.54 ± 0.00
CF-5	98.13 ± 1.39	100.0 ± 0.0	<u>95.54</u> ± 0.09	0.0 ± 0.0	0.56 ± 0.04	0.675 ± 0.027	1.57 ± 0.03
EU-10	100.0 ± 0.0	99.50 ± 0.02	93.61 ± 0.08	15.24 ± 1.08	0.40 ± 0.01	-0.349 ± 0.019	2.42 ± 0.11
CF-10	100.0 ± 0.0	99.98 ± 0.0	94.95 ± 0.05	11.61 ± 0.91	<u>0.41</u> ± 0.01	-0.060 ± 0.017	2.31 ± 0.03
SCRUB	100.0 ± 0.0	100.0 ± 0.0	95.37 ± 0.04	19.73 ± 1.92	0.47 ± 0.01	<u>-0.056</u> ± 0.008	3.49 ± 0.02
SALUN	<u>99.99</u> ± 0.01	100.0 ± 0.0	95.42 ± 0.12	0.01 ± 0.01	0.73 ± 0.04	0.936 ± 0.012	3.54 ± 0.11
ℓ_1 -sparse	100.0 ± 0.0	99.93 ± 0.02	94.90 ± 0.10	1.56 ± 0.09	0.47 ± 0.03	0.293 ± 0.012	2.96 ± 0.03
COLA	100.0 ± 0.0	100.0 ± 0.00	95.36 ± 0.06	<u>12.64</u> ± 0.92	0.44 ± 0.04	0.010 ± 0.006	4.91 ± 0.04
CIFAR-10 - ResNet-50							
Methods	UA	RA	TA	MIA	JSD	IDI	RTE (min)
Original	0.0	100.0	95.42	95.58	4.11	1.000	341.86
Retrain	100.0	100.0	95.49	14.92	0.0	0.0	312.24
FT	100.0 ± 0.0	<u>99.99</u> ± 0.0	95.28 ± 0.11	2.17 ± 1.28	0.73 ± 0.02	0.607 ± 0.009	14.50 ± 0.34
RL	100.0 ± 0.0	100.0 ± 0.0	95.56 ± 0.03	0.0 ± 0.0	0.99 ± 0.02	0.804 ± 0.006	6.26 ± 0.04
GA	100.0 ± 0.0	98.06 ± 0.34	92.07 ± 0.63	20.56 ± 3.87	0.66 ± 0.06	0.334 ± 0.023	8.69 ± 0.03
Bad-T	100.0 ± 0.0	99.94 ± 0.04	94.74 ± 0.24	49.95 ± 40.74	3.02 ± 0.64	1.153 ± 0.026	10.19 ± 0.32
EU-5	100.0 ± 0.0	100.0 ± 0.0	95.59 ± 0.08	0.0 ± 0.0	0.78 ± 0.08	1.047 ± 0.005	<u>4.86</u> ± 0.43
CF-5	<u>17.84</u> ± 0.93	100.0 ± 0.0	95.64 ± 0.11	0.0 ± 0.0	1.43 ± 0.04	0.906 ± 0.002	4.84 ± 0.10
EU-10	100.0 ± 0.0	100.0 ± 0.0	<u>95.51</u> ± 0.12	0.17 ± 0.05	0.65 ± 0.02	0.757 ± 0.011	6.92 ± 0.02
CF-10	100.0 ± 0.0	100.0 ± 0.0	95.49 ± 0.13	0.07 ± 0.03	0.67 ± 0.08	0.579 ± 0.009	7.09 ± 0.02
SCRUB	100.0 ± 0.0	100.0 ± 0.0	95.23 ± 0.20	<u>18.19</u> ± 0.10	0.59 ± 0.01	<u>0.067</u> ± 0.020	8.69 ± 0.03
SALUN	100.0 ± 0.0	99.67 ± 0.17	93.90 ± 0.48	1.58 ± 0.98	0.67 ± 0.03	0.832 ± 0.027	11.00 ± 0.06
ℓ_1 -sparse	100.0 ± 0.0	99.88 ± 0.06	94.49 ± 0.29	4.06 ± 0.91	0.47 ± 0.01	0.184 ± 0.023	12.33 ± 0.04
COLA	100.0 ± 0.0	<u>99.99</u> ± 0.0	95.45 ± 0.05	13.69 ± 0.84	<u>0.52</u> ± 0.02	0.019 ± 0.025	11.98 ± 0.03
CIFAR-10 - ViT							
Methods	UA	RA	TA	MIA	JSD	IDI	RTE (min)
Original	0.36	99.55	98.40	89.12	3.96	1.000	100.68*
Retrain	100.0	99.40	97.96	4.96	0.0	0.0	90.96*
FT	98.10 ± 0.24	99.85 ± 0.06	97.58 ± 0.36	21.14 ± 0.92	0.71 ± 0.13	-0.871 ± 0.141	130.13 ± 0.63
RL	97.88 ± 2.12	99.88 ± 0.01	99.01 ± 0.02	0.0 ± 0.0	0.74 ± 0.04	1.052 ± 0.011	65.45 ± 0.12
GA	100.0 ± 0.0	99.80 ± 0.03	98.49 ± 0.12	4.82 ± 0.98	0.39 ± 0.05	0.498 ± 0.025	68.32 ± 0.80
Bad-T	100.0 ± 0.0	99.55 ± 0.03	<u>98.40</u> ± 0.20	0.0 ± 0.0	0.84 ± 0.06	0.997 ± 0.016	100.90 ± 1.02
EU-5	100.0 ± 0.0	99.76 ± 0.01	98.80 ± 0.01	0.30 ± 0.01	0.28 ± 0.03	0.901 ± 0.006	<u>29.89</u> ± 0.09
CF-5	100.0 ± 0.0	99.76 ± 0.0	98.86 ± 0.02	0.35 ± 0.03	0.26 ± 0.01	0.941 ± 0.001	34.12 ± 0.09
EU-10	100.0 ± 0.0	99.72 ± 0.02	98.63 ± 0.04	0.64 ± 0.02	<u>0.23</u> ± 0.03	<u>0.268</u> ± 0.016	32.74 ± 0.19
CF-10	100.0 ± 0.0	99.77 ± 0.01	98.75 ± 0.02	0.64 ± 0.04	0.21 ± 0.02	0.377 ± 0.039	36.79 ± 0.15
SCRUB	100.0 ± 0.0	<u>99.66</u> ± 0.0	98.57 ± 0.01	94.74 ± 0.26	3.87 ± 0.07	0.907 ± 0.027	22.99 ± 0.24
SALUN	100.0 ± 0.0	99.78 ± 0.02	98.89 ± 0.02	0.01 ± 0.01	0.39 ± 0.05	1.066 ± 0.041	61.37 ± 0.10
ℓ_1 -sparse	100.0 ± 0.0	97.48 ± 0.27	95.78 ± 0.16	<u>3.89</u> ± 0.79	0.41 ± 0.03	-0.573 ± 0.290	51.44 ± 0.04
COLA	<u>99.44</u> ± 0.02	100.0 ± 0.0	98.82 ± 0.06	11.90 ± 1.36	0.63 ± 0.11	-0.067 ± 0.010	116.01 ± 0.96

Table 11: Single-class forgetting result on CIFAR-10 dataset across different model architectures. A better performance of an MU method corresponds to a smaller performance gap with Retrain (except RTE), with the top method in **bold** and the second best underlined. The * symbol indicated in RTE of Original and Retrain means that models are pretrained on ImageNet-21K and then finetuned on CIFAR-10, with the reported time reflecting only the finetuning process. In contrast, Original and Retrain without * are trained from scratch on CIFAR-10.

CIFAR-100 - ResNet-18							
Methods	UA	RA	TA	MIA	JSD	IDI	RTE (min)
Original	0.0	99.98	78.18	92.80	2.91	1.000	175.08
Retrain	100.0	99.96	79.48	2.00	0.0	0.0	171.27
FT	100.0 ± 0.0	99.97 ± 0.0	77.49 ± 0.14	0.07 ± 0.09	0.37 ± 0.01	0.610 ± 0.022	9.50 ± 0.03
RL	93.80 ± 0.75	<u>99.98</u> ± 0.0	<u>77.94</u> ± 0.10	0.0 ± 0.0	0.52 ± 0.01	0.467 ± 0.010	3.52 ± 0.0
GA	<u>99.93</u> ± 0.09	96.87 ± 0.52	69.87 ± 0.78	21.40 ± 2.04	1.18 ± 0.02	0.392 ± 0.021	5.32 ± 0.01
Bad-T	100.0 ± 0.0	<u>99.98</u> ± 0.0	77.66 ± 0.26	40.87 ± 36.87	2.53 ± 0.44	1.079 ± 0.024	5.78 ± 0.02
EU-5	100.0 ± 0.0	99.78 ± 0.01	75.01 ± 0.04	9.33 ± 0.75	0.66 ± 0.01	<u>0.064</u> ± 0.037	2.14 ± 0.0
CF-5	100.0 ± 0.0	99.97 ± 0.0	77.30 ± 0.28	<u>2.87</u> ± 0.66	0.40 ± 0.03	0.388 ± 0.010	2.14 ± 0.01
EU-10	100.0 ± 0.0	91.94 ± 0.08	72.84 ± 0.04	12.67 ± 0.47	0.53 ± 0.02	-0.221 ± 0.009	4.39 ± 0.02
CF-10	100.0 ± 0.0	99.89 ± 0.02	76.49 ± 0.02	7.07 ± 0.84	0.49 ± 0.01	0.175 ± 0.040	4.29 ± 0.04
SCRUB	100.0 ± 0.0	<u>99.98</u> ± 0.0	78.17 ± 0.04	0.07 ± 0.09	<u>0.31</u> ± 0.01	0.339 ± 0.069	2.27 ± 0.02
SALUN	95.73 ± 0.85	99.22 ± 0.13	74.20 ± 0.52	0.09 ± 0.02	0.65 ± 0.01	0.529 ± 0.022	4.63 ± 0.06
ℓ_1 -sparse	96.93 ± 0.19	98.90 ± 0.12	74.69 ± 0.06	6.60 ± 0.43	0.34 ± 0.01	0.334 ± 0.026	4.55 ± 0.01
COLA	100.0 ± 0.0	99.80 ± 0.00	76.48 ± 0.11	9.60 ± 1.31	0.26 ± 0.01	-0.037 ± 0.006	7.51 ± 0.02
CIFAR-100 - ResNet-50							
Methods	UA	RA	TA	MIA	JSD	IDI	RTE (min)
Original	0.0	99.98	79.84	91.60	3.43	1.000	345.54
Retrain	100.0	99.97	79.42	3.40	0.0	0.0	338.58
FT	99.33 ± 0.09	99.93 ± 0.03	77.71 ± 0.18	0.40 ± 0.16	0.57 ± 0.02	0.618 ± 0.018	16.34 ± 0.47
RL	100.0 ± 0.0	99.95 ± 0.02	<u>79.56</u> ± 0.04	0.0 ± 0.0	0.80 ± 0.0	0.649 ± 0.013	8.38 ± 0.14
GA	99.60 ± 0.43	98.00 ± 0.72	72.73 ± 1.16	13.33 ± 4.43	0.99 ± 0.04	0.526 ± 0.009	9.50 ± 0.54
Bad-T	100.0 ± 0.0	99.90 ± 0.10	77.53 ± 1.21	94.80 ± 2.75	3.98 ± 0.25	0.990 ± 0.033	12.69 ± 1.54
EU-5	100.0 ± 0.0	99.97 ± 0.01	78.31 ± 0.21	<u>1.20</u> ± 0.99	0.61 ± 0.04	0.520 ± 0.023	<u>6.81</u> ± 0.01
CF-5	100.0 ± 0.0	99.97 ± 0.01	78.98 ± 0.16	0.27 ± 0.09	0.50 ± 0.02	0.575 ± 0.016	6.82 ± 0.01
EU-10	100.0 ± 0.0	98.52 ± 0.14	75.66 ± 0.03	15.00 ± 1.45	0.69 ± 0.01	<u>0.050</u> ± 0.004	7.81 ± 0.01
CF-10	100.0 ± 0.0	99.95 ± 0.01	78.47 ± 0.10	5.87 ± 0.09	0.50 ± 0.02	0.302 ± 0.035	7.82 ± 0.02
SCRUB	100.0 ± 0.0	99.97 ± 0.0	79.61 ± 0.09	0.20 ± 0.16	<u>0.43</u> ± 0.02	0.620 ± 0.034	4.59 ± 0.13
SALUN	99.73 ± 0.38	<u>99.98</u> ± 0.0	79.51 ± 0.15	0.0 ± 0.0	0.80 ± 0.01	0.679 ± 0.010	12.83 ± 0.87
ℓ_1 -sparse	96.20 ± 0.16	99.42 ± 0.06	76.16 ± 0.31	2.60 ± 0.33	<u>0.43</u> ± 0.01	0.325 ± 0.018	15.78 ± 0.05
COLA	100.0 ± 0.0	99.90 ± 0.01	78.59 ± 0.28	10.27 ± 0.90	0.42 ± 0.02	0.016 ± 0.031	16.25 ± 0.10
CIFAR-100 - ViT							
Methods	UA	RA	TA	MIA	JSD	IDI	RTE (min)
Original	7.00	95.85	90.78	69.20	2.71	1.000	102.45*
Retrain	100.0	95.79	90.58	10.00	0.0	0.0	94.29*
FT	100.0 ± 0.0	99.79 ± 0.04	88.69 ± 0.11	14.80 ± 2.40	0.57 ± 0.03	-0.934 ± 0.011	140.61 ± 0.25
RL	99.19 ± 0.23	97.11 ± 0.02	92.28 ± 0.06	0.31 ± 0.01	0.82 ± 0.01	1.091 ± 0.031	73.12 ± 0.18
GA	100.0 ± 0.0	98.19 ± 0.20	90.59 ± 0.21	17.60 ± 4.78	0.31 ± 0.01	0.587 ± 0.011	75.22 ± 0.61
Bad-T	95.80 ± 0.08	95.88 ± 0.12	90.15 ± 0.02	0.0 ± 0.0	1.11 ± 0.14	1.213 ± 0.002	96.43 ± 0.01
EU-5	100.0 ± 0.0	97.59 ± 0.04	92.04 ± 0.02	7.10 ± 0.70	<u>0.27</u> ± 0.01	1.143 ± 0.008	<u>32.17</u> ± 0.02
CF-5	100.0 ± 0.0	97.81 ± 0.01	91.98 ± 0.05	6.93 ± 0.32	<u>0.27</u> ± 0.01	1.087 ± 0.050	36.73 ± 0.03
EU-10	100.0 ± 0.0	97.87 ± 0.01	91.45 ± 0.07	13.30 ± 1.97	0.36 ± 0.02	0.849 ± 0.012	34.23 ± 0.02
CF-10	100.0 ± 0.0	97.87 ± 0.01	91.61 ± 0.05	15.80 ± 0.80	0.32 ± 0.02	0.734 ± 0.011	39.12 ± 0.0
SCRUB	100.0 ± 0.00	96.95 ± 0.03	92.12 ± 0.06	17.00 ± 1.21	<u>0.27</u> ± 0.02	<u>0.037</u> ± 0.036	17.84 ± 0.13
SALUN	99.73 ± 0.31	98.32 ± 0.04	92.23 ± 0.05	0.47 ± 0.06	0.78 ± 0.02	1.123 ± 0.043	203.12 ± 0.51
ℓ_1 -sparse	100.0 ± 0.0	<u>96.37</u> ± 0.06	<u>90.92</u> ± 0.07	3.80 ± 1.62	0.23 ± 0.01	1.144 ± 0.002	56.93 ± 0.32
COLA	100.0 ± 0.0	99.76 ± 0.02	90.23 ± 0.04	12.00 ± 2.20	0.54 ± 0.01	-0.022 ± 0.016	112.58 ± 0.82

Table 12: Single-class forgetting result on CIFAR-100 dataset across different model architectures. A better performance of an MU method corresponds to a smaller performance gap with Retrain (except RTE), with the top method in **bold** and the second best underlined. The * symbol indicated in RTE of Original and Retrain means that models are pretrained on ImageNet-21K and then finetuned on CIFAR-100, with the reported time reflecting only the finetuning process. In contrast, Original and Retrain without are * trained from scratch on CIFAR-100.

CIFAR-10 - 2-class forgetting							
Methods	UA	RA	TA	MIA	JSD	IDI	RTE (min)
Original	0.0	100.0	95.76	91.10	3.55	1.000	170.32
Retrain	100.0	100.0	96.38	29.58	0.0	0.0	135.23
FT	<u>99.98</u> \pm 0.01	100.0 \pm 0.0	<u>96.36</u> \pm 0.09	0.96 \pm 0.53	0.58 \pm 0.08	0.750 \pm 0.009	5.92 \pm 0.09
RL	99.70 \pm 0.02	100.0 \pm 0.0	96.39 \pm 0.01	0.0 \pm 0.0	1.07 \pm 0.01	0.863 \pm 0.001	2.79 \pm 0.02
GA	99.07 \pm 0.38	99.43 \pm 0.13	94.83 \pm 0.22	<u>26.71</u> \pm 3.68	0.42 \pm 0.02	0.612 \pm 0.001	3.72 \pm 0.13
Bad-T	99.96 \pm 0.05	100.0 \pm 0.0	95.33 \pm 0.09	67.47 \pm 34.59	3.98 \pm 1.08	1.010 \pm 0.005	4.40 \pm 0.20
EU-5	100.0 \pm 0.0	100.0 \pm 0.0	96.48 \pm 0.06	0.06 \pm 0.03	0.57 \pm 0.05	0.624 \pm 0.001	1.39 \pm 0.02
CF-5	80.06 \pm 8.26	100.0 \pm 0.0	96.70 \pm 0.04	0.0 \pm 0.0	0.80 \pm 0.02	0.781 \pm 0.006	<u>1.41</u> \pm 0.05
EU-10	100.0 \pm 0.0	99.67 \pm 0.02	94.94 \pm 0.17	25.92 \pm 0.79	<u>0.35</u> \pm 0.01	-0.011 \pm 0.011	2.20 \pm 0.17
CF-10	100.0 \pm 0.0	99.67 \pm 0.02	94.94 \pm 0.17	21.20 \pm 1.43	<u>0.35</u> \pm 0.01	<u>0.221</u> \pm 0.007	2.19 \pm 0.14
SCRUB	<u>99.98</u> \pm 0.0	<u>99.99</u> \pm 0.0	96.31 \pm 0.08	46.74 \pm 5.31	1.47 \pm 0.10	0.374 \pm 0.005	3.27 \pm 0.01
SALUN	95.86 \pm 4.18	<u>99.99</u> \pm 0.01	96.27 \pm 0.11	0.04 \pm 0.01	0.89 \pm 0.05	0.951 \pm 0.019	3.17 \pm 0.02
ℓ_1 -sparse	99.91 \pm 0.05	99.98 \pm 0.0	96.47 \pm 0.09	1.57 \pm 0.11	0.50 \pm 0.02	0.560 \pm 0.004	2.62 \pm 0.06
COLA	100.0 \pm 0.0	99.92 \pm 0.0	96.41 \pm 0.15	31.40 \pm 2.98	0.26 \pm 0.01	0.011 \pm 0.029	4.59 \pm 0.02
CIFAR-100 - 5-class forgetting							
Methods	UA	RA	TA	MIA	JSD	IDI	RTE (min)
Original	0.0	99.98	77.95	95.00	3.18	1.000	175.08
Retrain	100.0	99.98	78.45	7.12	0.0	0.0	165.92
FT	100.0 \pm 0.0	99.93 \pm 0.06	<u>77.43</u> \pm 0.20	0.20 \pm 0.06	0.38 \pm 0.01	0.596 \pm 0.009	9.21 \pm 0.06
RL	98.61 \pm 0.22	99.98 \pm 0.0	77.78 \pm 0.19	0.0 \pm 0.0	0.71 \pm 0.01	0.613 \pm 0.008	3.39 \pm 0.09
GA	79.99 \pm 4.75	95.18 \pm 0.40	68.68 \pm 0.52	32.25 \pm 2.02	1.36 \pm 0.06	0.236 \pm 0.010	4.99 \pm 0.04
Bad-T	100.0 \pm 0.0	99.98 \pm 0.0	75.93 \pm 0.57	44.60 \pm 31.96	2.86 \pm 0.25	1.021 \pm 0.031	5.51 \pm 0.11
EU-5	100.0 \pm 0.0	99.75 \pm 0.02	75.14 \pm 0.12	12.40 \pm 0.26	0.54 \pm 0.01	<u>0.054</u> \pm 0.010	2.01 \pm 0.0
CF-5	100.0 \pm 0.0	<u>99.97</u> \pm 0.0	77.36 \pm 0.06	3.37 \pm 0.52	<u>0.36</u> \pm 0.02	0.319 \pm 0.011	<u>2.10</u> \pm 0.0
EU-10	100.0 \pm 0.0	91.76 \pm 0.12	73.24 \pm 0.11	21.96 \pm 0.49	0.48 \pm 0.01	-0.155 \pm 0.008	4.25 \pm 0.0
CF-10	100.0 \pm 0.0	99.88 \pm 0.01	76.59 \pm 0.24	10.69 \pm 1.29	0.40 \pm 0.01	0.087 \pm 0.019	4.29 \pm 0.01
SCRUB	100.0 \pm 0.0	<u>99.97</u> \pm 0.0	<u>77.64</u> \pm 0.11	0.95 \pm 0.35	0.56 \pm 0.03	0.289 \pm 0.015	2.27 \pm 0.03
SALUN	100.0 \pm 0.0	99.96 \pm 0.01	77.18 \pm 0.14	0.13 \pm 0.09	0.55 \pm 0.01	0.597 \pm 0.029	4.46 \pm 0.04
ℓ_1 -sparse	<u>98.63</u> \pm 0.37	97.50 \pm 0.14	73.46 \pm 0.25	12.35 \pm 0.82	0.38 \pm 0.01	0.196 \pm 0.011	4.19 \pm 0.01
COLA	100.0 \pm 0.0	99.82 \pm 0.0	77.47 \pm 0.26	11.16 \pm 0.54	0.29 \pm 0.01	0.044 \pm 0.010	7.31 \pm 0.02
CIFAR-100 - 20-class forgetting							
Methods	UA	RA	TA	MIA	JSD	IDI	RTE (min)
Original	0.0	99.97	78.03	95.04	3.15	1.000	175.08
Retrain	100.0	99.98	80.01	7.55	0.0	0.0	139.93
FT	<u>99.81</u> \pm 0.04	<u>99.97</u> \pm 0.00	79.11 \pm 0.35	0.22 \pm 0.05	0.37 \pm 0.01	<u>0.474</u> \pm 0.007	7.43 \pm 0.07
RL	95.77 \pm 0.09	99.98 \pm 0.01	78.42 \pm 0.05	0.0 \pm 0.0	0.63 \pm 0.01	1.207 \pm 0.004	2.94 \pm 0.01
GA	67.06 \pm 2.58	96.65 \pm 0.47	70.80 \pm 0.65	30.16 \pm 1.42	1.46 \pm 0.11	1.027 \pm 0.006	4.11 \pm 0.02
Bad-T	95.54 \pm 0.61	99.98 \pm 0.01	69.71 \pm 0.32	32.07 \pm 35.23	2.83 \pm 0.26	1.211 \pm 0.011	5.17 \pm 0.11
EU-5	100.0 \pm 0.0	99.82 \pm 0.02	76.89 \pm 0.03	14.50 \pm 0.54	0.52 \pm 0.01	0.807 \pm 0.003	<u>1.83</u> \pm 0.04
CF-5	100.0 \pm 0.0	99.96 \pm 0.02	<u>78.82</u> \pm 0.06	2.68 \pm 0.21	<u>0.33</u> \pm 0.01	1.060 \pm 0.008	1.80 \pm 0.03
EU-10	100.0 \pm 0.0	93.25 \pm 0.32	74.79 \pm 0.39	25.63 \pm 0.38	0.47 \pm 0.01	0.617 \pm 0.005	3.61 \pm 0.51
CF-10	100.0 \pm 0.0	99.91 \pm 0.01	78.39 \pm 0.24	13.57 \pm 0.32	0.39 \pm 0.01	0.889 \pm 0.005	3.68 \pm 0.16
SCRUB	95.03 \pm 0.75	99.90 \pm 0.00	77.61 \pm 0.07	0.93 \pm 0.13	0.38 \pm 0.01	0.997 \pm 0.007	2.14 \pm 0.02
SALUN	90.69 \pm 0.76	98.97 \pm 0.14	74.72 \pm 0.54	0.17 \pm 0.03	0.60 \pm 0.01	1.113 \pm 0.008	3.85 \pm 0.0
ℓ_1 -sparse	83.49 \pm 0.46	99.52 \pm 0.03	76.79 \pm 0.20	6.36 \pm 0.59	0.38 \pm 0.01	1.035 \pm 0.007	3.08 \pm 0.07
COLA	100.0 \pm 0.0	99.92 \pm 0.0	78.59 \pm 0.32	<u>11.52</u> \pm 0.39	0.24 \pm 0.01	0.007 \pm 0.010	6.97 \pm 0.01

Table 13: Multi-class forgetting on CIFAR-10 and CIFAR-100 datasets on ResNet-18 model. A better performance of an MU method corresponds to a smaller performance gap with Retrain (except RTE), with the top method in **bold** and the second best underlined.

ImageNet-1K - ResNet-50							
Methods	UA	RA	TA	MIA	JSD	IDI	RTE (min)
Original	11.72	87.45	76.11	61.69	3.73	1.000	2680.15
Retrain	100.0	88.80	75.88	9.41	0.0	0.0	2661.90
FT	100.0 _{±0.0}	88.52 _{±0.0}	<u>76.16</u> _{±0.01}	8.24 _{±1.23}	<u>0.24</u> _{±0.01}	0.102 _{±0.026}	140.04 _{±1.42}
RL	<u>99.96</u> _{±0.03}	86.46 _{±0.07}	<u>75.23</u> _{±0.01}	0.23 _{±0.01}	1.57 _{±0.03}	1.002 _{±0.007}	200.73 _{±1.87}
GA	100.0 _{±0.0}	80.77 _{±0.22}	71.49 _{±0.10}	4.20 _{±0.46}	0.42 _{±0.03}	0.328 _{±0.023}	212.14 _{±2.61}
Bad-T	98.01 _{±0.02}	84.03 _{±0.03}	73.42 _{±0.03}	69.13 _{±12.57}	3.51 _{±0.41}	1.152 _{±0.072}	211.52 _{±0.96}
EU-5	100.0 _{±0.0}	79.62 _{±0.0}	71.22 _{±0.13}	13.33 _{±1.53}	0.26 _{±0.01}	0.183 _{±0.028}	193.38 _{±0.78}
CF-5	100.0 _{±0.0}	84.31 _{±0.08}	74.16 _{±0.06}	10.21 _{±5.33}	0.23 _{±0.01}	0.701 _{±0.014}	81.53 _{±0.56}
EU-10	100.0 _{±0.0}	71.84 _{±0.03}	65.78 _{±0.02}	16.65 _{±1.91}	0.35 _{±0.04}	<u>-0.051</u> _{±0.021}	193.79 _{±0.47}
CF-10	100.0 _{±0.0}	80.87 _{±0.04}	72.34 _{±0.08}	13.99 _{±5.41}	0.25 _{±0.01}	0.608 _{±0.012}	82.29 _{±0.34}
SCRUB	99.28 _{±0.07}	<u>88.39</u> _{±0.04}	76.51 _{±0.03}	7.42 _{±0.51}	0.25 _{±0.01}	0.517 _{±0.011}	426.04 _{±2.98}
SALUN	89.67 _{±0.27}	86.25 _{±0.15}	75.54 _{±0.10}	0.50 _{±0.09}	0.88 _{±0.01}	0.343 _{±0.017}	793.82 _{±3.32}
ℓ_1 -sparse	97.57 _{±0.61}	85.33 _{±0.07}	74.77 _{±0.03}	<u>8.84</u> _{±1.39}	0.32 _{±0.02}	0.239 _{±0.031}	226.74 _{±1.35}
COLA	100.0 _{±0.0}	87.93 _{±0.05}	76.15 _{±0.04}	9.95 _{±1.21}	<u>0.24</u> _{±0.01}	0.040 _{±0.042}	171.44 _{±0.75}

ImageNet-1K - ViT							
Methods	UA	RA	TA	MIA	JSD	IDI	RTE (min)
Original	2.48	98.18	80.59	71.00	4.45	1.000	1943.69*
Retrain	100.0	98.33	80.42	8.09	0.0	0.0	1920.77*
FT	96.39 _{±0.01}	98.85 _{±0.03}	80.93 _{±0.06}	3.88 _{±0.33}	0.65 _{±0.02}	0.937 _{±0.009}	281.73 _{±2.30}
RL	98.33 _{±0.02}	98.99 _{±0.07}	81.65 _{±0.07}	0.0 _{±0.0}	2.13 _{±0.15}	1.152 _{±0.033}	150.32 _{±4.31}
GA	100.0 _{±0.0}	97.04 _{±0.01}	<u>80.17</u> _{±0.04}	8.26 _{±2.14}	0.52 _{±0.23}	0.674 _{±0.021}	193.73 _{±2.23}
Bad-T	98.21 _{±0.03}	<u>97.85</u> _{±0.07}	80.58 _{±0.03}	0.0 _{±0.0}	2.62 _{±0.06}	1.312 _{±0.015}	721.15 _{±5.23}
EU-5	100.0 _{±0.0}	93.82 _{±0.02}	80.00 _{±0.01}	4.74 _{±1.33}	0.63 _{±0.02}	0.519 _{±0.008}	300.55 _{±0.76}
CF-5	98.75 _{±0.0}	96.57 _{±0.01}	80.09 _{±0.04}	4.49 _{±0.34}	0.64 _{±0.01}	0.731 _{±0.024}	122.39 _{±0.53}
EU-10	100.0 _{±0.0}	87.33 _{±0.10}	76.26 _{±0.13}	8.09 _{±0.20}	0.36 _{±0.02}	-2.662 _{±0.231}	345.37 _{±0.70}
CF-10	<u>99.95</u> _{±0.01}	93.86 _{±0.02}	78.69 _{±0.01}	7.68 _{±1.11}	0.72 _{±0.03}	<u>0.009</u> _{±0.021}	<u>140.11</u> _{±0.49}
SCRUB	100.0 _{±0.00}	98.84 _{±0.02}	81.62 _{±0.01}	3.19 _{±0.91}	1.062 _{±0.03}	-0.846 _{±0.032}	404.02 _{±2.96}
SALUN	94.64 _{±0.76}	98.13 _{±0.21}	80.74 _{±0.05}	0.13 _{±0.01}	1.83 _{±0.09}	0.980 _{±0.065}	321.13 _{±2.75}
ℓ_1 -sparse	93.55 _{±0.62}	94.69 _{±0.37}	78.84 _{±0.10}	2.98 _{±0.33}	<u>0.49</u> _{±0.01}	0.831 _{±0.022}	717.42 _{±3.21}
COLA	100.0 _{±0.0}	96.42 _{±0.03}	79.28 _{±0.21}	<u>8.02</u> _{±1.36}	0.59 _{±0.02}	0.006 _{±0.007}	501.12 _{±2.17}

Table 14: 5-class forgetting results on ImageNet-1K dataset across different model architectures. A better performance of an MU method corresponds to a smaller performance gap with Retrain (except RTE), with the top method in **bold** and the second best underlined. The * symbol indicated in RTE of Original and Retrain means that models are pretrained on ImageNet-21K and then finetuned on ImageNet-1K, with the reported time reflecting only the finetuning process. In contrast, Original and Retrain without * are trained from scratch on ImageNet-1K.

CIFAR-10 - ResNet-18							
Methods	UA	RA	TA	MIA	JSD	IDI	RTE (min)
Original	0.0	100.0	95.54	92.90	0.09	1.000	170.32
Retrain	3.94	100.0	95.26	75.12	0.0	0.0	152.87
FT	5.03 \pm 0.40	98.95 \pm 0.21	92.94 \pm 0.26	83.52 \pm 0.58	0.07 \pm 0.11	<u>-0.069</u> \pm 0.013	8.11 \pm 0.03
RL	4.77 \pm 0.27	99.92 \pm 0.0	93.54 \pm 0.04	22.47 \pm 1.19	0.38 \pm 0.02	0.084 \pm 0.030	2.75 \pm 0.01
GA	2.86 \pm 0.76	98.37 \pm 0.71	91.90 \pm 0.70	85.49 \pm 2.17	0.09 \pm 0.01	0.924 \pm 0.028	4.31 \pm 0.03
Bad-T	5.47 \pm 1.05	<u>99.87</u> \pm 0.05	91.51 \pm 0.61	39.53 \pm 3.43	0.27 \pm 0.03	0.939 \pm 0.053	4.78 \pm 0.09
EU-10	3.16 \pm 0.19	98.68 \pm 0.08	93.07 \pm 0.12	<u>83.40</u> \pm 0.21	<u>0.06</u> \pm 0.01	-0.110 \pm 0.013	<u>2.13</u> \pm 0.05
CF-10	2.71 \pm 0.24	99.11 \pm 0.06	<u>93.47</u> \pm 0.15	84.33 \pm 0.05	0.05 \pm 0.01	0.219 \pm 0.029	2.10 \pm 0.06
SCRUB	<u>4.31</u> \pm 1.50	96.21 \pm 1.70	88.83 \pm 1.86	37.88 \pm 7.65	0.56 \pm 0.09	0.322 \pm 0.016	3.37 \pm 0.05
SALUN	2.74 \pm 0.30	97.77 \pm 0.04	91.68 \pm 0.44	83.52 \pm 2.20	0.10 \pm 0.03	0.861 \pm 0.012	5.69 \pm 0.04
ℓ_1 -sparse	5.47 \pm 0.22	96.66 \pm 0.07	91.31 \pm 0.25	77.12 \pm 0.21	0.09 \pm 0.01	-0.157 \pm 0.026	3.03 \pm 0.04
COLA+	3.90 \pm 0.08	99.24 \pm 0.17	93.23 \pm 0.09	83.48 \pm 0.10	<u>0.06</u> \pm 0.01	0.024 \pm 0.010	7.80 \pm 0.02
CIFAR-100 - ResNet-18							
Methods	UA	RA	TA	MIA	JSD	IDI	RTE (min)
Original	0.0	99.98	78.09	95.82	0.56	1.000	175.08
Retrain	23.10	99.98	77.78	39.72	0.0	0.0	170.31
FT	17.44 \pm 1.12	98.46 \pm 0.24	70.99 \pm 0.45	67.35 \pm 0.53	0.46 \pm 0.02	0.311 \pm 0.034	8.40 \pm 0.13
RL	24.67 \pm 0.42	<u>99.66</u> \pm 0.0	73.10 \pm 0.49	2.13 \pm 0.17	0.84 \pm 0.02	-0.246 \pm 0.056	2.95 \pm 0.03
GA	11.73 \pm 1.43	95.21 \pm 0.78	68.38 \pm 1.03	74.97 \pm 1.10	0.65 \pm 0.01	0.704 \pm 0.039	4.66 \pm 0.03
Bad-T	64.35 \pm 7.44	99.07 \pm 0.56	53.05 \pm 2.53	11.85 \pm 5.93	1.51 \pm 0.16	1.003 \pm 0.006	5.04 \pm 0.05
EU-10	24.15 \pm 0.09	90.15 \pm 0.08	72.25 \pm 0.36	59.47 \pm 0.39	0.27 \pm 0.01	0.404 \pm 0.085	<u>2.31</u> \pm 0.02
CF-10	20.40 \pm 0.20	95.06 \pm 0.24	74.44 \pm 0.23	62.18 \pm 0.27	<u>0.25</u> \pm 0.01	0.464 \pm 0.061	2.30 \pm 0.02
SCRUB	3.47 \pm 2.85	97.77 \pm 2.31	71.89 \pm 2.87	71.49 \pm 4.15	0.37 \pm 0.02	0.528 \pm 0.013	3.59 \pm 0.05
SALUN	32.77 \pm 1.20	99.87 \pm 0.02	71.97 \pm 0.37	3.32 \pm 0.28	0.81 \pm 0.02	-0.226 \pm 0.078	5.99 \pm 0.09
ℓ_1 -sparse	22.83 \pm 0.15	88.94 \pm 0.41	69.54 \pm 0.73	62.36 \pm 0.37	0.26 \pm 0.01	0.634 \pm 0.072	3.37 \pm 0.03
COLA+	<u>23.50</u> \pm 0.16	93.78 \pm 0.07	<u>73.15</u> \pm 0.59	<u>59.58</u> \pm 0.24	0.24 \pm 0.01	0.078 \pm 0.013	10.2 \pm 0.16

Table 15: Random data forgetting on CIFAR-10 and CIFAR-100 datasets on ResNet-18 model. A better performance of an MU method corresponds to a smaller performance gap with Retrain (except RTE), with the top method in **bold** and the second best underlined.

Method	Block 1	Block 2	Block 3	Block 4	Block 5	IDI
Original	0.002	0.002	0.003	0.006	0.006	0.005
Retrain	0.001	0.003	0.003	0.006	0.007	0.007
FT	0.001	0.002	0.004	0.010	0.008	0.007
RL	0.002	0.004	0.005	0.003	0.005	0.004
GA	0.001	0.001	0.004	0.006	0.011	0.013
l1-sparse	0.001	0.000	0.002	0.007	0.007	0.011
SCRUB	0.001	0.005	0.003	0.004	0.005	0.007
SALUN	0.002	0.001	0.003	0.005	0.012	0.011

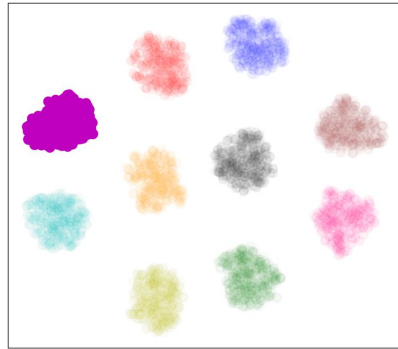
Table 16: Standard Deviation of Figure 4 - (CIFAR-10, ResNet-18)

Method	Block 1	Block 2	Block 3	Block 4	Block 5	Block 6	IDI
Original	0.003	0.002	0.009	0.007	0.013	0.008	0.011
Retrain	0.001	0.003	0.001	0.008	0.005	0.007	0.009
FT	0.003	0.005	0.008	0.015	0.011	0.012	0.019
RL	0.005	0.005	0.007	0.003	0.008	0.004	0.009
GA	0.002	0.001	0.003	0.011	0.010	0.013	0.018
l1-sparse	0.002	0.004	0.002	0.004	0.021	0.015	0.023
SCRUB	0.000	0.004	0.004	0.023	0.028	0.031	0.060
SALUN	0.001	0.000	0.006	0.005	0.020	0.011	0.019

Table 17: Standard Deviation of Figure 4 - (CIFAR-10, ResNet-50)

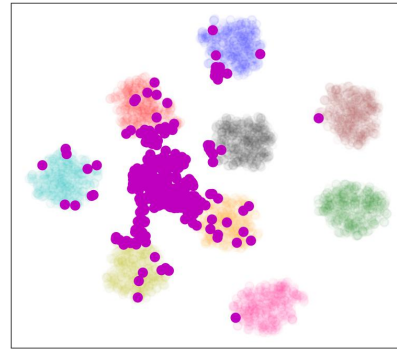
Method	Ratio 1:5	Ratio 1:20	Ratio 1:99
FT	0.013	0.008	0.019
RL	0.016	0.007	0.009
GA	0.020	0.008	0.018
CF-10	0.007	0.016	0.035
SALUN	0.023	0.025	0.019
SCRUB	0.006	0.013	0.023

Table 18: Standard Deviation of Figure 13



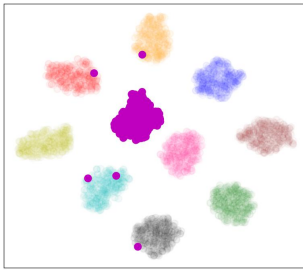
IDI: **1.000**

(a) Original



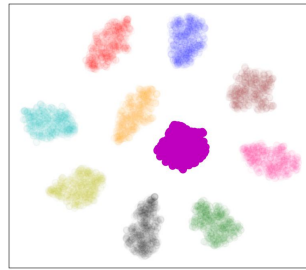
IDI: **0.000**

(b) Retrain



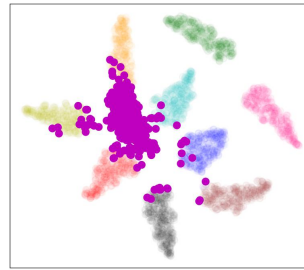
IDI: **0.671±0.008**

(c) FT



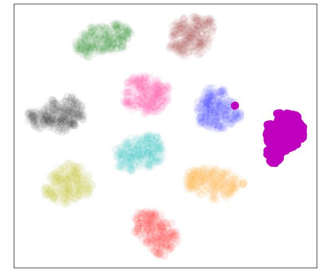
IDI: **0.830±0.005**

(d) RL



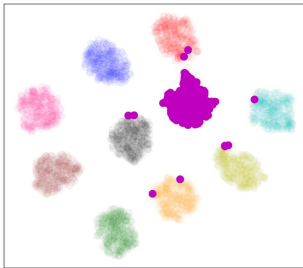
IDI: **0.334±0.014**

(e) GA



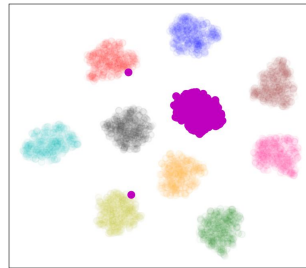
IDI: **1.014±0.004**

(f) Bad-T



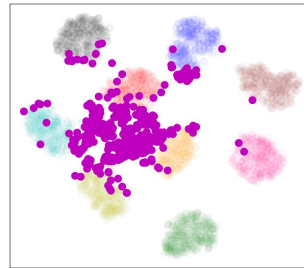
IDI: **0.528±0.005**

(g) EU-5



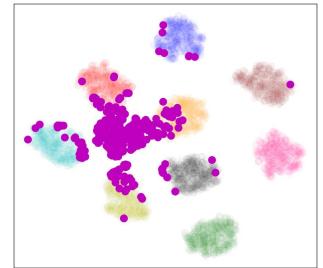
IDI: **0.675±0.027**

(h) CF-5



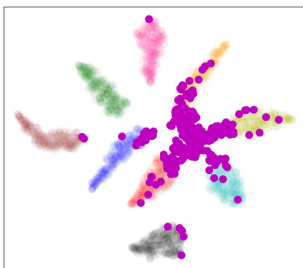
IDI: **-0.349±0.019**

(i) EU-10



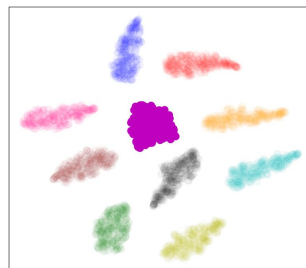
IDI: **-0.060±0.017**

(j) CF-10



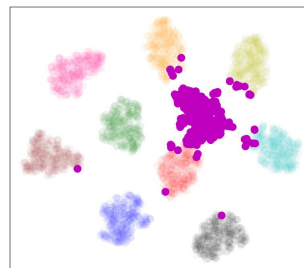
IDI: **-0.056±0.008**

(k) SCRUB



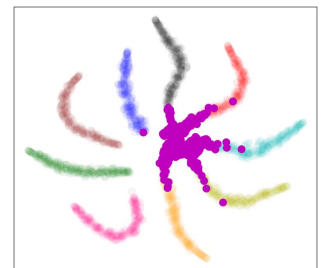
IDI: **0.936±0.012**

(l) SALUN



IDI: **0.293±0.012**

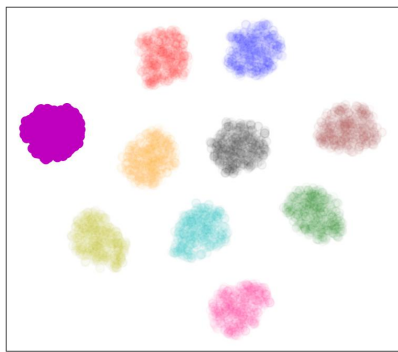
(m) ℓ_1 -sparse



IDI: **0.010±0.006**

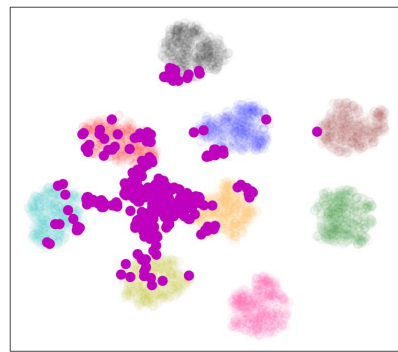
(n) COLA

Figure 14: t-SNE visualizations of features of Original, Retrain, and unlearned models (FT, RL, GA, Bad-T, EU-5, CF-5, EU-10, CF-10, SCRUB, SALUN, ℓ_1 -sparse, and COLA) on CIFAR-10 with ResNet-18. The forgetting class is represented in purple, while rest of the points represents the remaining class.



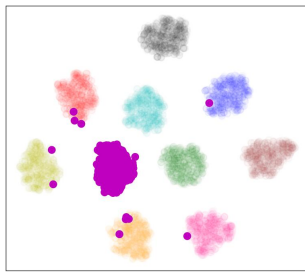
IDI: **1.000**

(a) Original



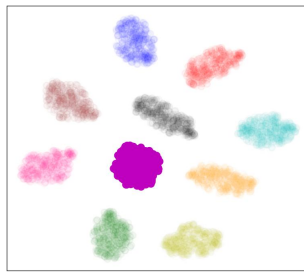
IDI: **0.000**

(b) Retrain



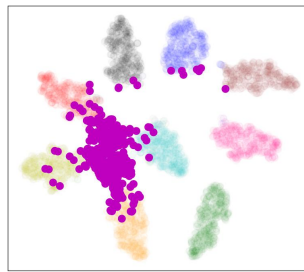
IDI: **0.607±0.009**

(c) FT



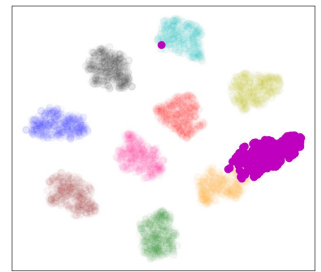
IDI: **0.804±0.006**

(d) RL



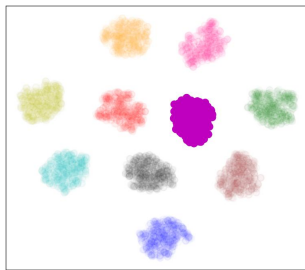
IDI: **0.334±0.023**

(e) GA



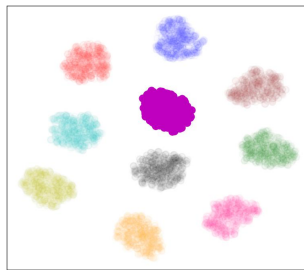
IDI: **1.153±0.026**

(f) Bad-T



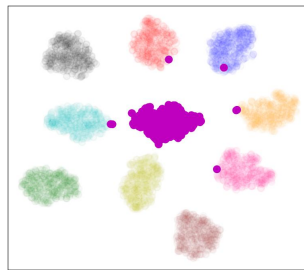
IDI: **1.047±0.005**

(g) EU-5



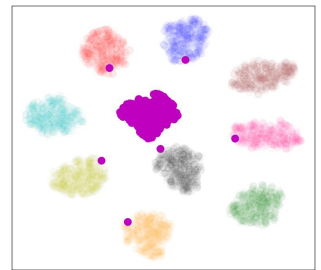
IDI: **0.906±0.002**

(h) CF-5



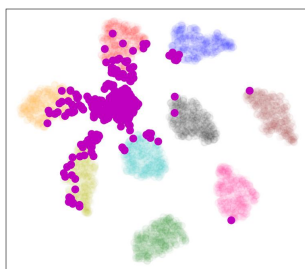
IDI: **0.757±0.011**

(i) EU-10



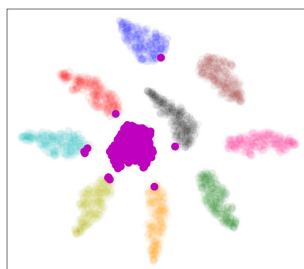
IDI: **0.579±0.009**

(j) CF-10



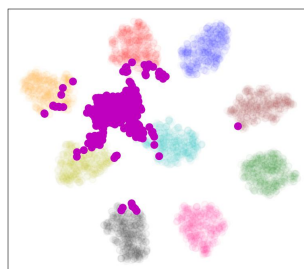
IDI: **0.067±0.020**

(k) SCRUB



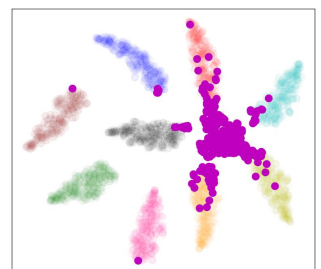
IDI: **0.832±0.027**

(l) SALUN



IDI: **0.184±0.023**

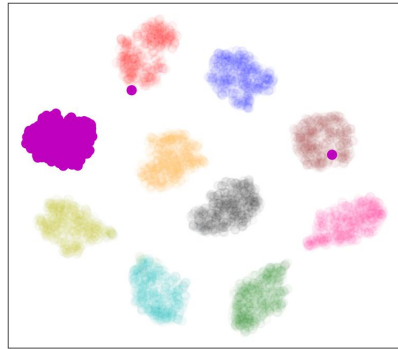
(m) ℓ_1 -sparse



IDI: **0.019±0.025**

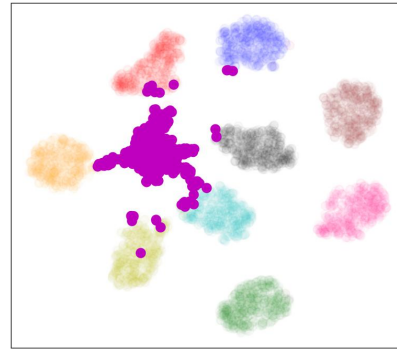
(n) COLA

Figure 15: t-SNE visualizations of feature of Original, Retrain, and unlearned models (FT, RL, GA, Bad-T, EU-5, CF-5, EU-10, CF-10, SCRUB, SALUN, ℓ_1 -sparse, and COLA) on CIFAR-10 with ResNet-50. The forgetting class is represented in purple, while rest of the points represents the remaining class.



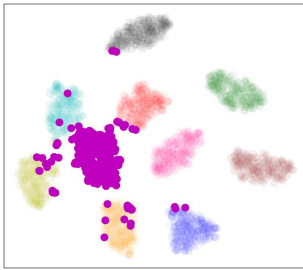
IDI: 1.000

(a) Original



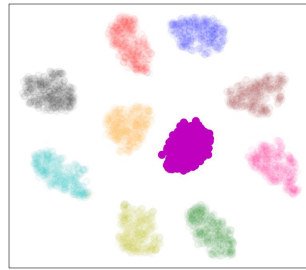
IDI: 0.000

(b) Retrain



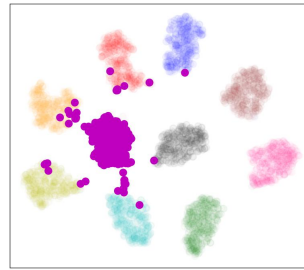
IDI: -0.871 ± 0.141

(c) FT



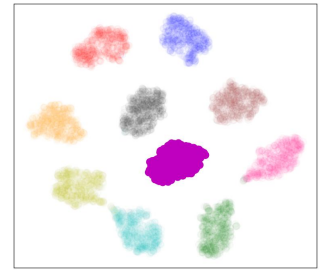
IDI: 1.052 ± 0.011

(d) RL



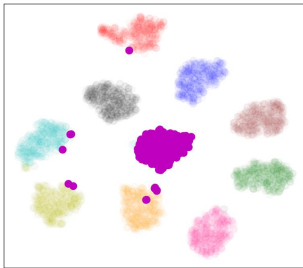
IDI: 0.498 ± 0.025

(e) GA



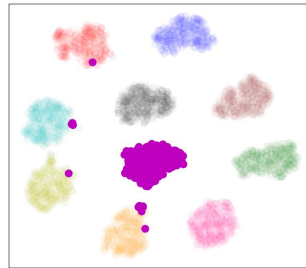
IDI: 0.997 ± 0.016

(f) Bad-T



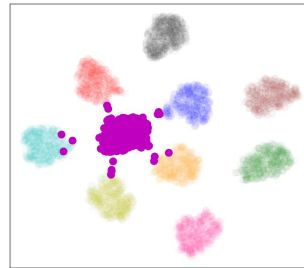
IDI: 0.901 ± 0.006

(g) EU-5



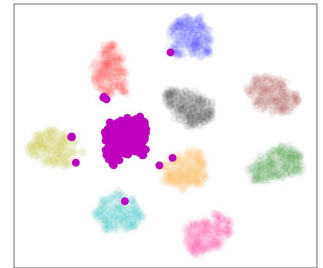
IDI: 0.941 ± 0.001

(h) CF-5



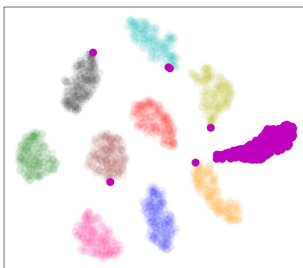
IDI: 0.268 ± 0.016

(i) EU-10



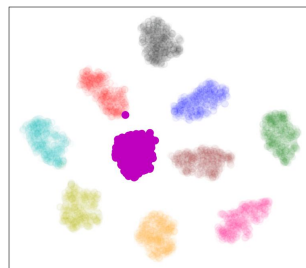
IDI: 0.377 ± 0.039

(j) CF-10



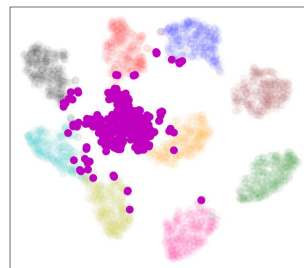
IDI: 0.907 ± 0.027

(k) SCRUB



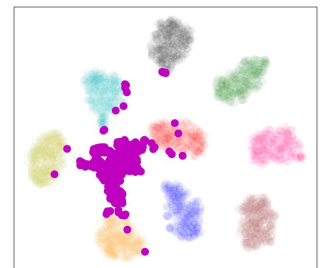
IDI: 1.066 ± 0.041

(l) SALUN



IDI: -0.573 ± 0.290

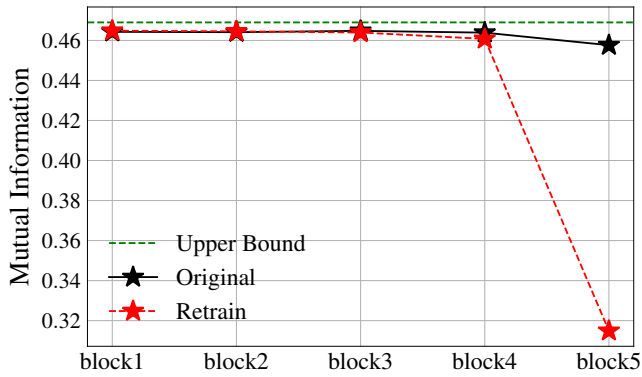
(m) ℓ_1 -sparse



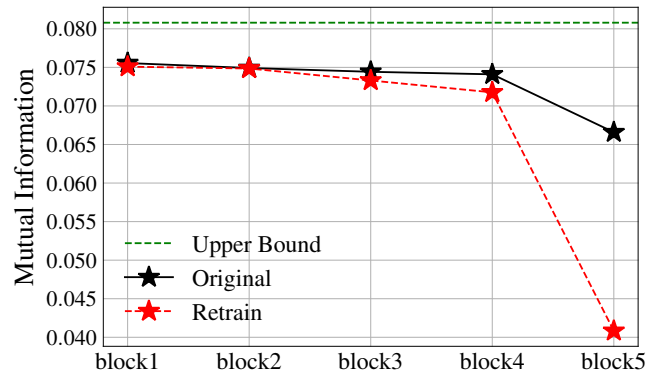
IDI: -0.067 ± 0.010

(n) COLA

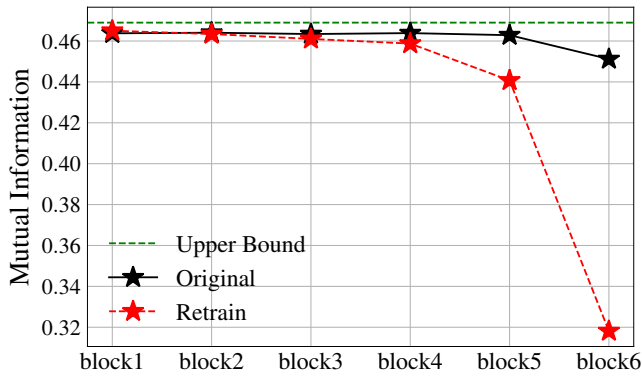
Figure 16: t-SNE visualizations of features of Original, Retrain, and unlearned models (FT, RL, GA, Bad-T, EU-5, CF-5, EU-10, CF-10, SCRUB, SALUN, ℓ_1 -sparse, and COLA) on CIFAR-10 with ViT. The forgetting class is represented in purple, while rest of the points represents the remaining class.



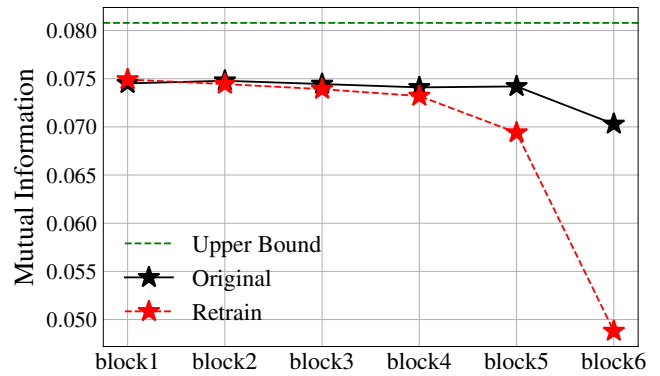
(a) CIFAR-10 - ResNet-18



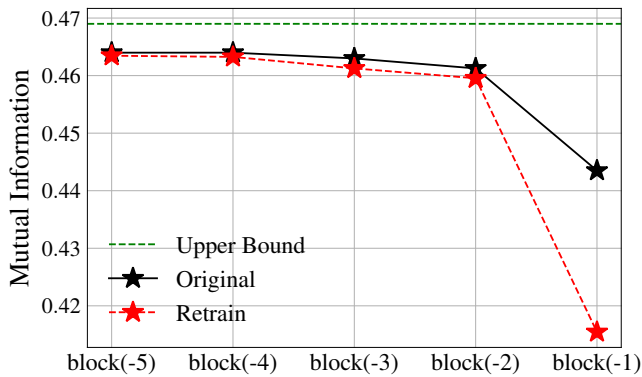
(b) CIFAR-100 - ResNet-18



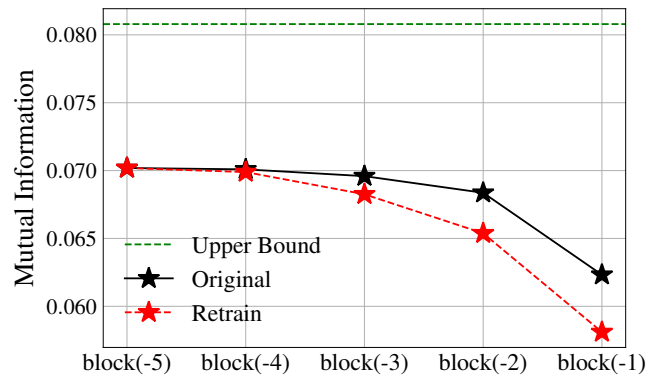
(c) CIFAR-10 - ResNet-50



(d) CIFAR-100 - ResNet-50



(e) CIFAR-10 - ViT



(f) CIFAR-100 - ViT

Figure 17: Mutual information curves across various datasets and model architectures. It illustrates the estimated mutual information $I(\mathbf{Z}_\ell; Y)$ of the features from the ℓ -th layer \mathbf{Z}_ℓ and the binary label Y , computed by the InfoNCE loss. 'block(-k)' means the k block front from the last layer.

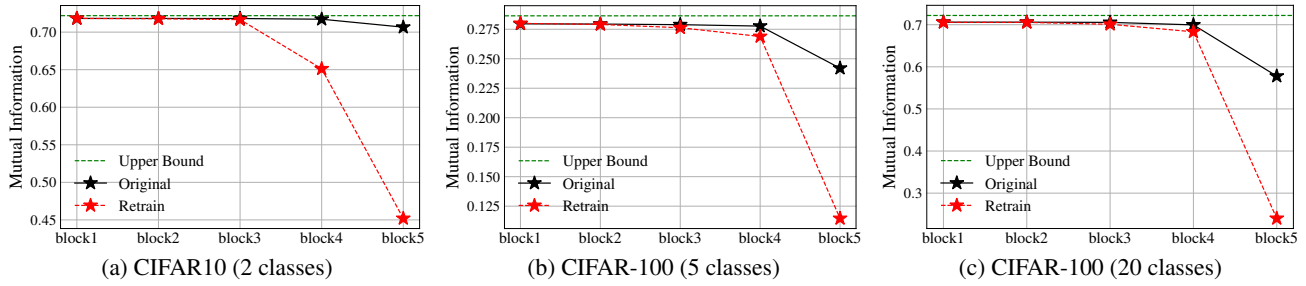


Figure 18: Mutual information curves for multiple class unlearning in ResNet-18 architecture. It illustrates the estimated mutual information $I(\mathbf{Z}_\ell; Y)$ of the features from the ℓ -th layer \mathbf{Z}_ℓ and the binary label Y , computed by the InfoNCE loss.

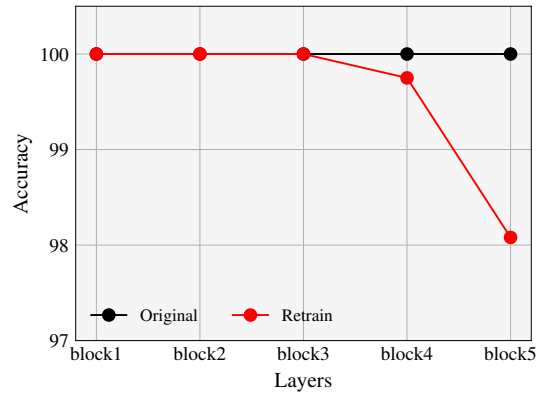


Figure 19: Binary train accuracy on CIFAR-10 in single-class forgetting with retain and forget sets. Interestingly, it shows similar results with mutual information plots shown Figure 17.

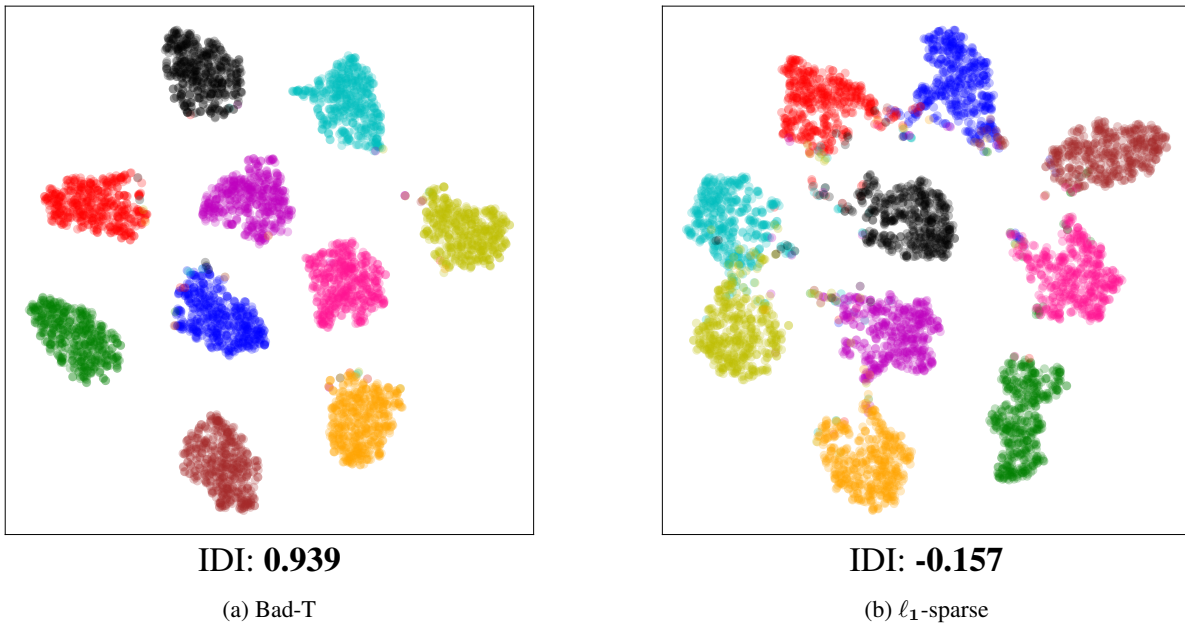


Figure 20: t-SNE visualizations of features of forget samples of Bad-T and ℓ_1 -sparse in a random data forgetting task on (CIFAR-10, ResNet-18). The clusters of ℓ_1 -sparse are more dispersed than those of Bad-T.